THE (α, Be^7) REACTION IN LIGHT ELEMENTS AT ENERGIES BELOW 42 MEV

by

CHARLES OLIVER HOWER, JR

A thesis submitted in partial fulfillment

of the requirements for the degree of

DOCTOR OF PHILOSOPHY

UNIVERSITY OF WASHINGTON

1962

Approved by C. W. Fairhall

Department Chemistry

Date 3/15/62

UNIVERSITY OF WASHINGTON

Date: February 27, 1962

We have carefully read the thesis entitled The (α, Be^7) Reaction in Light Elements at Energies Below 42 Mev.

submitted by Charles Oliver Hower in partial fulfillment of the requirements of the degree of Doctor of Philosophy and recommend its acceptance. In support of this recommendation we present the following joint statement of evaluation to be filed with the thesis.

The thesis presents the results of a careful investigation using radiochemical techniques of nuclear reactions which lead to the production of Be^7 fragments. Elements in the region between carbon and aluminum were bombarded with helium ions of up to 42 Mev in energy. Very little is known about the production of fragments heavier than alpha particles at energies as low as 40 Mev and the mechanism by which these fragments are produced is not clear. Several approaches to the understanding of the nature of nuclear reactions which produce Be^7 were taken. One approach was an examination of the angular distribution of the Be^7 fragments; in the favorable case of the $Al^{27}(\alpha, Be^7)Na^{24}$ the angular distribution of residual Na^{24} nuclei was examined also. The results are not unambiguously clear but they strongly support the hypothesis that the reaction proceeds through a compound nucleus. A second approach was the determination of the energies of the emitted Be^7 fragments. This was done by measurement of their ranges in metal foils. (The range-energy relation of beryllium ions in the foils was measured for the first time by a technique involving inelastic scattering of helium ions from beryllium metal.) The spectrum of kinetic energies of the Be^7 fragments was that which would be expected by evaporation from a compound nucleus. The third approach was the measurement of the excitation functions of Be^7 production in the various elements. These excitation functions agreed with expectations based on the compound nucleus mechanism. The conclusion is that most, if not all, of the observed Be^7 fragments are produced in an evaporation process from a compound nucleus.

THESIS READING COMMITTEE: W. Fairhall

Isaac Halpern

C. C. Lingafelter

In presenting this thesis in partial fulfillment of the requirements for an advanced degree at the University of Washington I agree that the Library shall make it freely available for inspection. I further agree that permission for extensive copying of this thesis for scholarly purposes may be granted by my major professor, or, in his absence, by the Director of Libraries. It is understood that any copying or publication of this thesis for financial gain shall not be allowed without my written permission.

Signature Charles O. Hower

Date March 15, 1962

TABLE OF CONTENTS

Table of Contents, continued.

LIST OF TABLES

LIST OF FIGURES

List of Figures, continued

List of Figures, continued

CHAPTER I

INTRODUCTION

Nuclear reactions at medium energies usually yield as products light particles, seldom heavier than He^4, and a heavy product not far removed in mass from the target nucleus. In recent years reactions have been observed which leave as the light product a particle heavier than He^4. An example is the production of Li^8 from proton and deuteron bombardment of several elements throughout the periodic table. Another example is Be^7 production from the helium ion bombardment of oxygen and aluminum. Such reactions have received little attention and are not well characterized. The interesting feature is the identification of a reaction product which is considerably heavier than He^4 and yet has a small mass compared with the target nucleus. Such a product will be referred to as a "heavy" fragment. The term is introduced only for convenience and no implication is intended that a heavy fragment is necessarily different in principle from a He^4 fragment or lighter particle.

Heavy fragment formation has been frequently observed in high energy reactions ranging from 4 Bev down to medium energies. Li^8 fragments make easily recognized tracks in a nuclear emulsion and its presence in cosmic ray stars has been the subject of many

investigations (17-207), (31-188). Munir (25-355) and Katcoff (21-905) have used the emulsion technique to measure the energy distribution of Li^8 fragments produced by high energy protons. Cross sections for the formation of He^6 from several elements bombarded by protons in the Bev range are reported by Rowland and Wolfgang (30-175). The first study of Be^7 production at high energies was made by Marquez and Perlman (24-953). They determined cross sections for 335 Mev protons incident on Be, C, Al, Cu, Ag and Au. Subsequent measurements of Be^7 cross sections in the energy range 300 Mev to 4 Bev have been made in several experiments (1-1319), (3-1), (8-902), (13-727), (14-263). The possibility that heavy fragments are left as the residues of spallation processes can be eliminated in most of these observations.

Heavy fragment production was apparently first observed by S. C. Wright (32-742) who studied the production of Li^8 from proton and deuteron bombardment of C, N, Ne, A, Kr and Xe. Wright used a proportional counter for the identification of the Li^8 fragments and measured cross sections in the bombarding energy range 30 Mev to 190 Mev. Bouchard (6-160), in work done at this laboratory, used radiochemical techniques to measure excitation functions for the reactions $Al^{27}(He^4, Be^7)Na^{24}$ and $O^{16}(He^4, Be^7)C^{13}$. Lindsay (22-2168) has extended Bouchard's cross section measurements

to Mg, Al, Ti, Co and Cu in the energy range 30 Mev to 42 Mev. Nicholson and Hower (26-18), have used a counter technique to detect Li and Be fragments from the helium ion bombardment of carbon and aluminum. Zafiratos (33) has used counters to study the (He^4, Li^6) reaction on N^{14}. The energy spectrum of the Li^6 fragments has two high energy groups and a continuum of low energy fragments. The two high energy groups show the characteristics of a direct interaction.

Only three nuclides in the mass range 4 to 10 are easily detected radiochemically. He^6, Li^8 and Be^7 are radioactive and have decay characteristics that make them amenable to observation. All other nuclides in this region are either stable or have very short half-lives. Since most of the work done on heavy fragments has relied on radiochemical techniques or on the unique decay properties of Li^8, the fact that other nuclides have not been observed is simply a reflection of the fact that they have not been looked for. It is therefore reasonable to assume that heavy fragments are not limited to He^6, Li^8 and Be^7, but instead have a continuous range of mass values in the region above He^4. In fact, the production of stable nuclides may be expected to be more probable because of the generally more favorable Q values for reactions which yield stable products.

Unfortunately, there are very few investigations at high energies and

none at medium energies which are rich enough in detail to test adequately the correspondence between observation and theory. It would be interesting to know if heavy fragment production can be accomodated by the present state of nuclear reaction theory.

Nuclear reaction mechanisms are conveniently divided into two groups, the compound nucleus mechanism and direct interactions. The concept of the compound nucleus was first proposed by Niels Bohr in 1936 (5-344) in order to account for the observation of resonances in the interaction of low energy neutrons with many elements. It has proved to be a durable idea. In compound nucleus theory a reaction is divided into two steps. The first step is the amalgamation of the incident particle with the target nucleus to form a compound system, that is, the compound nucleus. The kinetic energy of the incident particle, plus its contribution to the binding energy of the system, excites the compound nucleus to some energy above its ground state. The second step is the decay of the compound nucleus as it seeks to relieve itself of the excitation energy brought in by the incident particle. De-excitation is usually accomplished by particle emission if the excitation energy exceeds the binding energy of a nucleon. This is often referred to as particle "evaporation."

Further theoretical treatment assumes that the energy of the incident particle is distributed among all the nucleons of the system so

that a thermodynamic equilibrium is attained. The decay of the compound nucleus is now independent of its mode of formation and depends only on the dynamics of the system. By making estimates of the density of energy states in the nuclides involved, the course of this decay can be predicted. This is called the statistical theory of nuclear reactions. It requires that a nuclear reaction proceed on a relatively slow time scale, that is, the duration of the interaction is very long compared with the transit time of the incident particle across a nuclear diameter.

By contrast, a direct interaction proceeds on a relatively fast time scale. The incident particle interacts with a single nucleon or group of nucleons in the target nucleus. There is an exchange of momentum or particles or both, and the resulting products proceed on their separate courses. The initial interaction is not immediately communicated to all the nucleons of the system and therefore a compound nucleus has no part in the reaction. It is not always easy to distinguish experimentally between a direct interaction and compound nucleus formation, and frequently both concepts are needed in order to interpret the results of a single experiment.

The classification of reaction mechanisms into two unrelated groups is largely artificial, a result of the fact that theory is not well defined between the extremes of direct interaction and compound nucleus

formation. Nevertheless, it is still fruitful to review experimental results within the framework of these two theoretical approaches. If direct interactions are responsible for heavy fragment formation their study could supply information on the clustering of nucleons within the nucleus. They could also be used as a tool to study energy levels in light nuclei. On the other hand, heavy fragment reactions may go through a compound nucleus. This in itself is an interesting possibility, and in addition offers the hope of gaining a better understanding of the nature of the compound nucleus.

The purpose of this work is to study in detail several reactions which yield Be^{7} as the light product with special emphasis on determining the mechanism of the reaction.

CHAPTER II

EXPERIMENTAL METHODS

A. General Considerations.

There are two common ways of determining the mechanisms of nuclear reactions. One way is to measure the angular distribution of reaction products with respect to the beam of incident particles. A compound nucleus reaction generally has an angular distribution symmetric about 90° in the center-of-mass coordinate system. This is because an evaporated particle cannot distinguish between the backward and forward directions. The angular distribution need not be isotropic, and in fact will usually show maxima about 0° and 180° due to considerations of angular momentum conservation. A direct interaction will usually show a diffraction pattern in its angular distribution, an asymmetry about 90°, and, generally, a much greater yield in the forward hemisphere than in the backward hemisphere.

The second means of establishing a reaction mechanism is to look at the energy spectrum of the products. A compound nucleus reaction will exhibit an energy spectrum characteristic of an evaporation process, tending to favor products with low kinetic energies. A direct interaction, however, generally involves energy levels near

the ground states of the product nuclei and therefore tends to give products with high kinetic energies.

In addition, the study of excitation functions can supply clues to the reaction mechanism which, although in themselves inconclusive, may help to fortify conclusions drawn from other experiments.

With these considerations in mind, it was decided to measure the angular distribution and energy distribution of Be^7 fragments from the helium ion bombardment of several light elements. The radiochemical approach, using standard catcher foil techniques, was used because of its obvious advantage over counter systems in being able to detect low energy fragments at backward angles. Targets of carbon, oxygen and aluminum were chosen for their ease of preparation and because Bouchard's work indicated cross sections were high enough to make the experiments feasible. Targets much heavier than aluminum have yields that are too low to be useful. Cross section measurements were extended to carbon, nitrogen, fluorine, and neon.

B. Experimental Set-up.

Figures 1 and 2 show the arrangement of target and catcher foils used in the angular and energy distribution experiments. The assembly was made to fit in the target box of the University of Washington cyclotron where it could be exposed to 42.5 Mev helium ions. Silver

catcher foils were placed in cylindrical geometry about the target in such a way that the entire solid angle was covered. After a run the foils were removed and cut into annuli corresponding to appropriate angular ranges. Be^7 was isolated from the catchers chemically and counted. Range distribution measurements were made by substituting a stack of 2.45 mg/cm^2 gold foils for silver foils over a chosen angular range. The number of gold foils that a fragment went through determined its energy. In practice, a range distribution and angular distribution were done simultaneously during any run in order to conserve cyclotron time. Range data were summed to obtain a corresponding angular measurement.

The helium ion beam was collimated to a 1/4 inch diameter, which produced an uncertainty in the angular relations ranging from $\pm$ 4.5° at 10° to $\pm$ 1.5° at 70°. The beam was monitored by means of an electrical integrating system. A chemical monitor was used in some runs. Aluminum foil was placed over the carbon block and Na^{22} was counted to establish the relative exposure between different runs. The center of the catcher foils was taken as the point at which the helium ion beam impinged upon them. Since the target assembly was in the fringing field of the cyclotron magnet this point was not necessarily the center of the Be^7 fragment angular distribution as the magnetic field

FIGURE 1

Drawing of the support system for targets and catcher foils. Catcher foils were placed in cylindrical geometry around the target in such a manner as to cover the entire solid angle. Targets were held on the front side of the target support with a small aluminum block, not shown. Some dimensions are distorted for the sake of clarity.

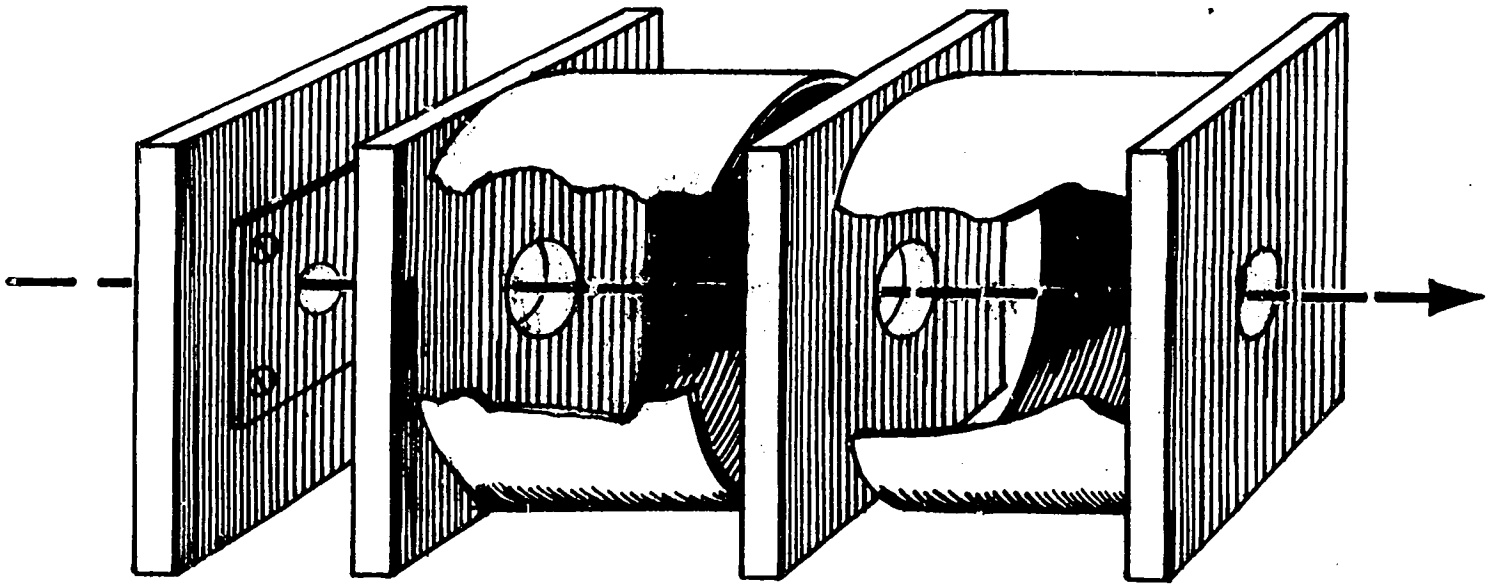

1/4" Cu COLLIMATOR

BACK CATCHER

TARGET SUPPORT

FRONT CATCHER

FIGURE 2

Top view of experimental set-up showing dimensional relations.

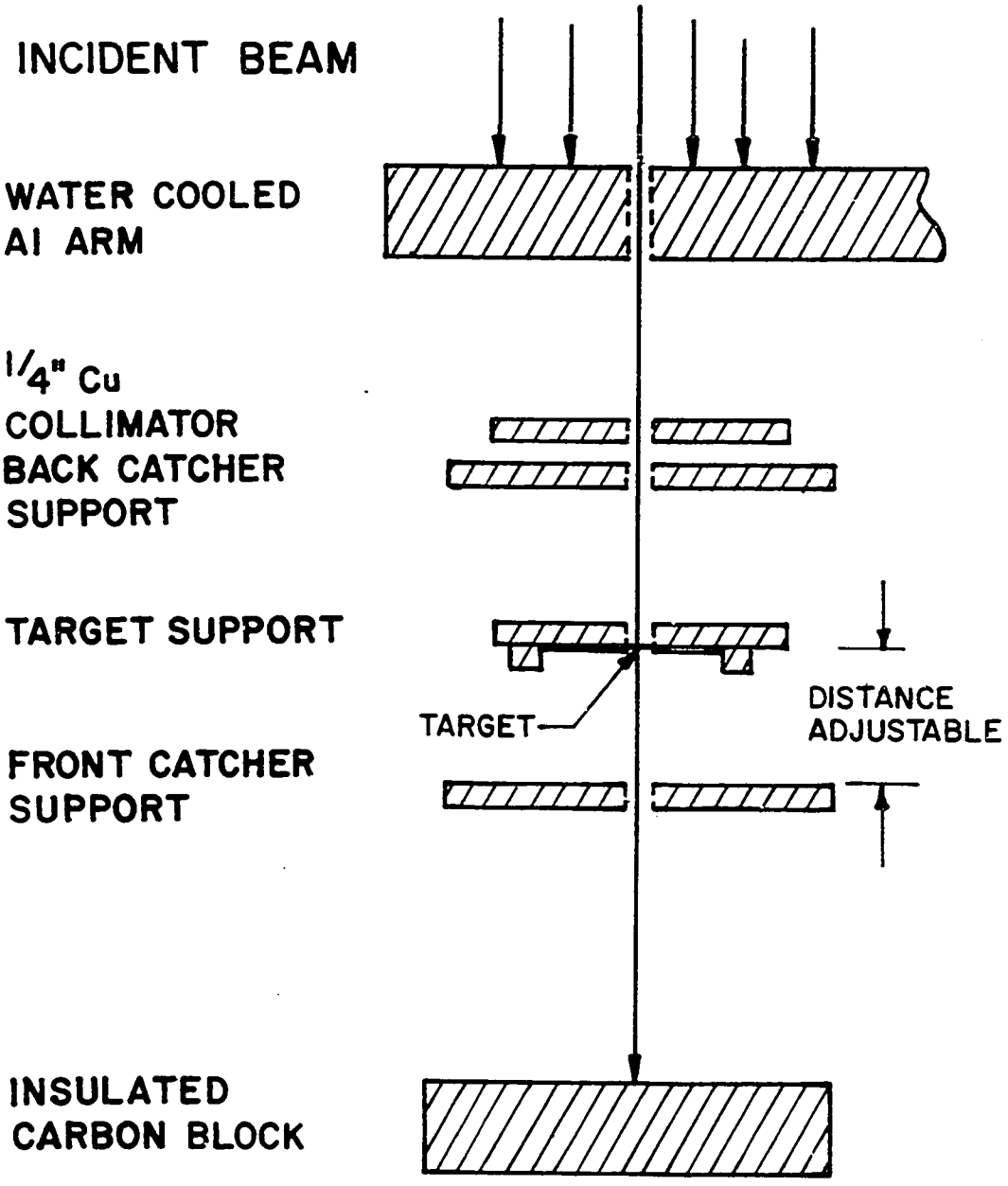
INCIDENT BEAM
WATER COOLED
Al ARM
1/4" Cu
COLLIMATOR
BACK CATCHER
SUPPORT
TARGET SUPPORT
TARGET
DISTANCE
ADJUSTABLE
FRONT CATCHER
SUPPORT
INSULATED
CARBON BLOCK

1/2 SCALE

would not influence the trajectories of the Be^7 ions and He ions to the same extent. This possibility was checked by dividing some annuli in half along the vertical axis and counting each half separately. No left-right asymmetry in counting rates was observed and it was concluded that the influence of the magnetic field on the Be^7 angular distributions could be safely ignored.

C. Targets.

Carbon targets were prepared by painting a colloidal suspension of graphite in alcohol (Dag 154, Acheson Colloids Company, Port Huron, Michigan) on glass slides. After drying, the graphite film was peeled from the glass under water, mounted, and baked at 500° C to remove impurities.

Oxygen targets were made by vacuum evaporation of MoO_3 onto a thin gold backing. MoO_3 was selected as the vehicle for oxygen because of the ease in preparing thin, uniform targets and because of the high ratio of oxygen to metal atoms. It was found that gentle heating of the evaporated deposit was necessary to produce an adhering film.

Commercially prepared foils were used for the aluminum targets.

D. Chemistry.

The chemical procedures for the isolation of Be^7 were the same as those used by Bouchard (6-160). They consisted essentially of H_2S

and $Fe(OH)_3$ scavenging steps, followed by repeated precipitation of $Be(OH)_2$ from an ammoniacal EDTA solution containing holdback carriers. The beryllium was finally precipitated and weighed as $BaBeF_4$. The samples were wrapped in small pieces of aluminum foil for counting.

The quantitative nature of the last precipitation step was demonstrated by tracer analysis. A quantity of carrier free Be^7 was prepared by bombarding a lithium target with deuterons. The target was dissolved in HCl and the slightly acidic solution was passed through a Dowex 50 resin column. Be was eluted with HCl. After waiting several days for short lived species to decay away, the sample was subjected to gamma ray spectrum analysis. The 0.48 Mev gamma ray of Be^7 was the only activity observed. The activity of the sample was measured, 10 mg of Be carrier were added, and the Be was precipitated in the usual manner as $BaBeF_4$. After drying and mounting, the activity was measured again and found to agree with the original value within experimental error, about 5%.

E. Counting.

Be^7 decays by K-capture, most of the transitions going to the ground state of Li^7. About 12% of the decays go to the first excited state of Li^7 which leads to a 0.477 Mev gamma ray. The half-life is

53 days, long enough to try the patience of even the most leisurely investigator.

The samples were placed in a two inch well crystal and counted with a Nuclear Chicago, Model 1810, single channel pulse height analyzer. The discriminators of the analyzer were set to pass only pulses corresponding to the energy range 0.43 to 0.53 Mev. This procedure gave a background counting rate of about 12 counts per minute, which made possible the collection of reasonable statistics on net counting rates as low as 1 c/m. The energy calibration and efficiency of the counting system were frequently checked against the 0.51 Mev annihilation quanta of a Na^{22} standard. The efficiency was assumed to be constant between 0.48 and 0.51 Mev.

The identification of Be^{7} was accomplished in three different ways. First, the chemistry is very specific for Be. Second, the decay was always followed for a sufficient length of time to establish the half-life. The samples from one particular run were followed for 200 days and the half-lives were established at 53 ± 2 days. No tails were observed within the limitations imposed by counting statistics. Third, pulse height analysis was always made on samples that showed sufficient activity. This was done with a two inch well crystal and an RCL 128 channel analyzer. Spectra were compared with the pure Be^{7} source, prepared from deuteron bombardment of lithium, which was

described in Section D. An additional test of purity was made on one of the samples derived from a MoO_3 target. This sample was counted once and then subjected to further chemical purification. When it was counted again the decrease in activity matched the decrease in chemical yield, indicating that only Be^7 was present.

F. Data Reduction.

The decay curves from each run were extrapolated back to zero time, taken as the end of bombardment, and the resulting activities were normalized to a 100% chemical yield. A blank run, to be described in the following chapter, indicated the presence of background activity. This activity was subtracted from all the data points.

Range data in gold were obtained, as described in Section B, for targets of carbon, oxygen, and aluminum. The Be^7 activity in each gold foil was plotted against the total thickness of gold that the fragments traversed. This was converted to a plot of relative activity versus Be^7 fragment energy by use of the experimentally determined range-energy function given in Figure 24 of Appendix I. Energy distributions were corrected for degradation of the fragments within the target by addition of the estimated energy loss in the target. This correction was never more than 0.5 Mev and was usually less.

The activity within each angular range was divided by the solid

angle subtended by the area of each annulus in order to obtain counts per minute per unit steradian. Center-of-mass correction factors were then applied to convert the data from the laboratory to the C.M. coordinate system. The tables of Marion, Arnette and Owens (23-1) were very helpful in making these conversions. The C.M. correction factors were, of course, determined from the energy of the Be^7 fragments. Since the energy of the fragments was found to extend over a considerable range of values, the Be^7 activity at each angle really represents a spectrum of energies. There is, therefore, an uncertainty introduced into the angular distributions. Fortunately, the angular distributions in the C.M. system were found to be rather insensitive to the C.M. corrections used, and even in the most critical case, that of oxygen, the uncertainty is less than the experimental error for 75% of the Be^7 fragments. This assumes that the energy distribution in the C.M. system does not change much with angle.

In order to translate the range distributions of Be^7 fragments into an energy distribution it is necessary to know the range-energy relationship for Be^7 ions in gold. Since this function had never been measured, and since available estimates are quite divergent, it was necessary to determine the range-energy relationship for Be^7. This was done by making the appropriate measurements on elastically scattered Be^9 recoils to obtain a range-energy curve for Be^9 ions in

gold. The data of L. C. Northcliffe (28-1744) on B^{10} and B^{11} ranges indicate that Be^{7} and Be^{9} fragments with the same energy differ in range by only 3%. This small correction was ignored. The range-energy experiment is described in detail in Appendix I.

G. Cross Sections.

Excitation functions were determined for Be^{7} production from helium ion bombardment of carbon, nitrogen, oxygen, fluorine and neon. Graphite targets, as described above, were used for carbon. Nitrogen and neon were bombarded as gases. Oxygen and fluorine targets were made by evaporating alcohol slurries of CuO and PbF_2 on silver foil. The "stacked chamber" apparatus designed by Ball (2-35) was used for the gas targets. The stacked foil technique was used for the solid targets. The foil stack was placed in the target position of the angular distribution assembly. This assured that a well collimated and easily monitored beam was incident on the stack. Silver foils were always used for the catchers and beam degraders. A guard foil was placed between the beam and the first target foil of the stack to exclude any Be^{7} that might have been produced in the collimators. The beam was monitored by feeding the suitably amplified beam current to an Esterline Angus chart recorder. The chemical separations and counting procedures were the same as those used in the angular distribution and energy distribution experiments.

CHAPTER III

DATA

A. Oxygen

The possible kinetic energies of Be^7 fragments from oxygen as a function of angle are shown in Figure 3. The upper curve is calculated on the basis of a 42.5 Mev incident helium ion and the Q value for the reaction O^{16} (He^4, Be^7) C^{13} when both products are formed in their ground states. The lower curve is determined by the energy that the Be^7 fragment must have in order to surmount the coulomb barrier. The effective barrier was arbitrarily taken as

$$2/3\ V = \frac{2/3\ Z_{Be^7}\ Z_t\ e^2}{(R_{Be^7} + R_t)}$$

The subscript t refers to the target element. Nuclear radii were obtained from $R = r_o A^{1/3}$ with $r_o = 1.3 \times 10^{-13}$ cm. All coulomb barriers were calculated in this manner. Appendix III contains a table of Q values and coulomb barrier heights which were used in this work. The area between the curves in Figure 3 represents the domain of possible energy values of Be^7 fragments.

Figure 4 gives the measured energy distribution of Be^7 fragments in the laboratory system within the angular range 20° to 30°. In

FIGURE 3

The possible energy values of Be^{7} fragments from oxygen as a function of angle. The upper curve is calculated on the basis of a 42.5 Mev incident helium ion and the Q value for the reaction O^{16} (He^{4}, Be^{7}) C^{13} when both products are formed in their ground states. The lower curve was calculated by assuming an effective coulomb barrier 2/3 that of the maximum coulomb barrier.

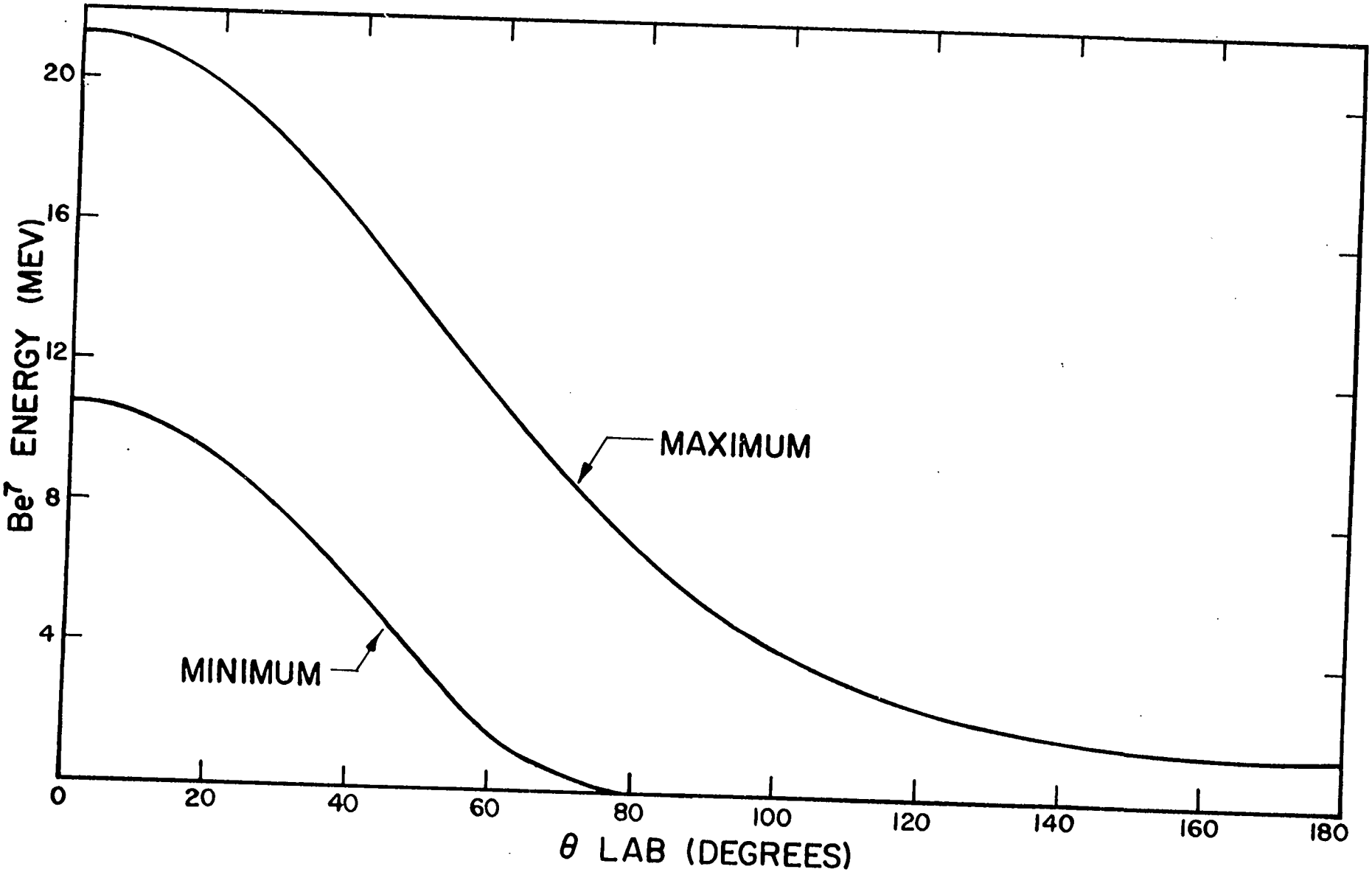
20
16
12
8
4
Be⁷ ENERGY (MEV)
MAXIMUM
MINIMUM
0
20
40
60
80
100
120
140
160
180
θ LAB (DEGREES)

FIGURE 4

The energy distribution of Be^7 fragments from oxygen in the laboratory system in the angular range 20° to 30°. The error limits derive from counting statistics and an assumed 3% error in chemical yield factors. The target was 1.2 mg/cm^2 of MoO_3. The vertical, hatched bars indicate the expected limits of the energy distribution as ascertained from Figure 3. The thickness of the bars indicates the extent of kinematic broadening over the angular range 20° to 30°.

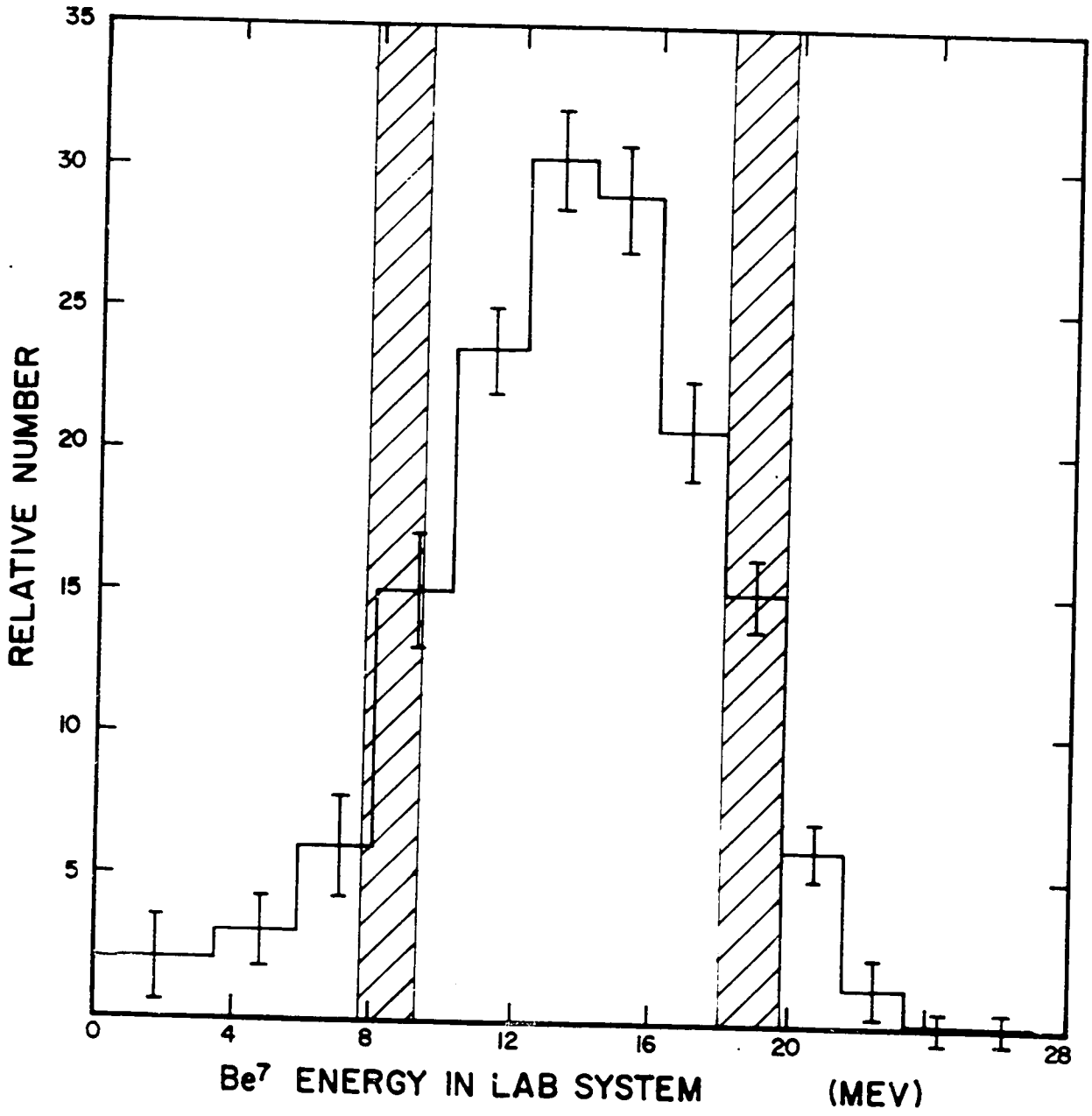
35
30
25
20
15
10
5
0
4
8
12
16
20
28
RELATIVE NUMBER
Be7 ENERGY IN LAB SYSTEM
(MEV)

Figure 5 the same data are plotted in the C.M. system. Figure 6 presents energy distribution data in the C.M. system within the angular range 0° to 16°. The resolution of these measurements is determined largely by the thickness of the gold catcher foils. The energy spread expected from the target thickness and the angular range is less than the energy loss in a single gold foil. From Figure 3 we can estimate the extreme limits of the energy distribution within the angular range 20° to 30° as being 8 Mev to 20 Mev. This agrees quite well with the observed distribution in Figure 4. Be^{7} fragments with kinetic energies below 6 or 7 Mev are most likely contributed by large angle scattering events in the target. However, in transforming these data into the C.M. system it was necessary to use a mean angle to represent the angular interval of 20° to 30°. This accounts for the apparent excess of high and low energy fragments observed in Figure 5. This point applies to all energy distribution data plotted in the C.M. system. The mean angle was always chosen so as to divide the angular interval into equal units of solid angle. Thus, for the 20° to 30° interval the mean angle was 25.4°.

Two conclusions are evident. First, the energy distribution is rather broad, indicating that C^{13} can be left in a number of excited states. Second, C^{13} is preferentially left in its higher excited states

FIGURE 5

The energy distribution of Be^7 fragments from oxygen in the C.M. system in the angular range 20° to 30°. The data are the same as those of Figure 4. The abscissa at the top of the figure gives the excitation energy left in the product nuclei for any given Be^7 energy. Since the highest reported bound state of Be^7 is at 0.43 Mev, this may be regarded as the excitation energy left in the C^{13} nucleus. The smooth curve is a fit to

$$\frac{dP}{dE} = (E - V_{eff}) \exp\left(-\frac{E}{T}\right).$$

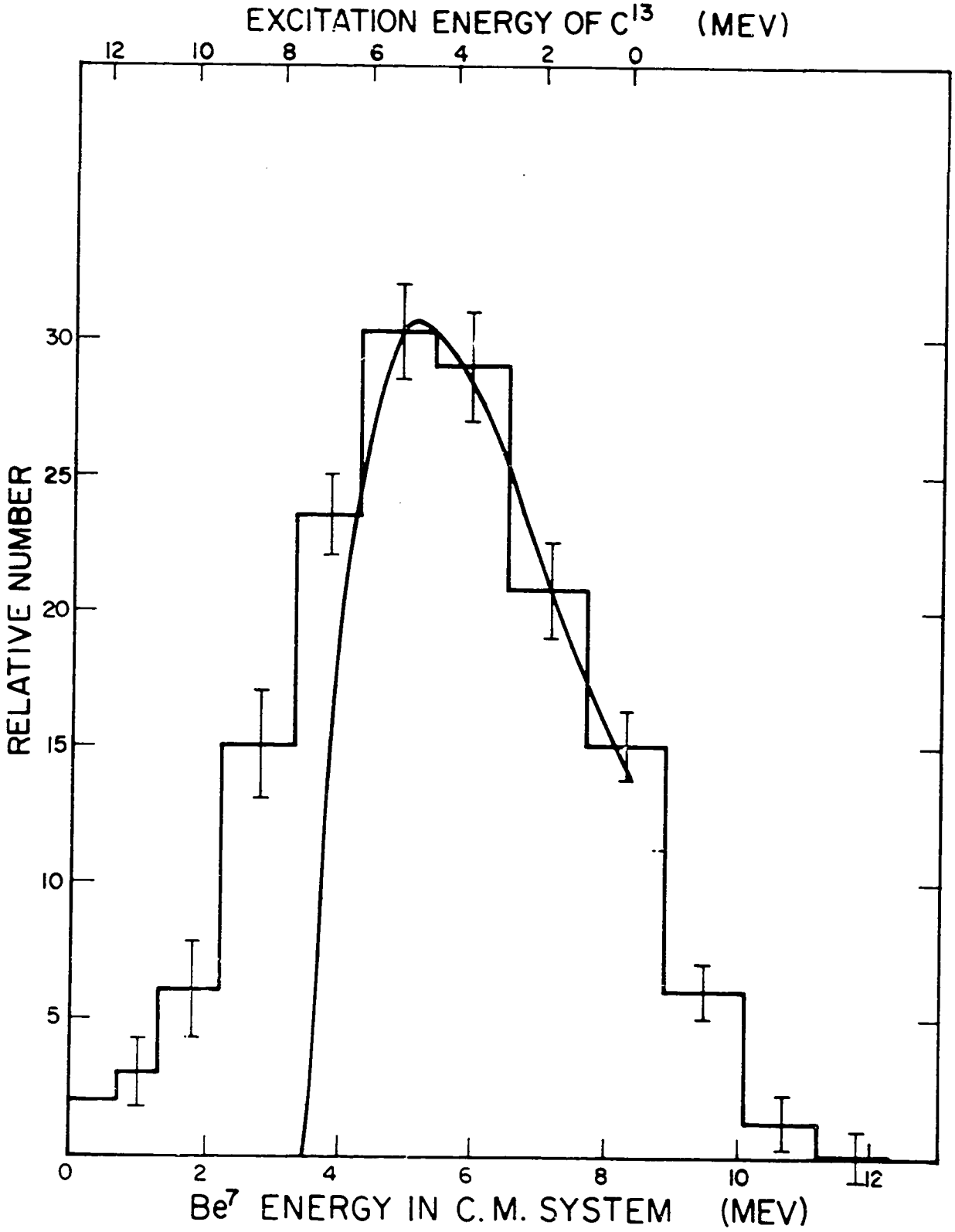
EXCITATION ENERGY OF C^{13} (MEV)
12
10
8
6
4
2
0
RELATIVE NUMBER
30
25
20
15
10
5
0
2
4
6
8
10
12
Be^7 ENERGY IN C.M. SYSTEM (MEV)

FIGURE 6

The energy distribution of Be^7 fragments from oxygen in the C.M. system in the angular range 0° to 16°. The abscissa at the top of the figure gives the excitation energy left in the product nuclei for any given Be^7 energy. Since the highest reported bound state of Be^7 is at 0.43 Mev, this may be regarded as the excitation energy left in the C^{13} nucleus. Error limits, omitted from run number 2, derive from counting statistics and an assumed 3% error in chemical yield factors. The target thicknesses were 0.6 mg/cm^2 and 0.9 mg/cm^2 for runs number 1 and 2, respectively.

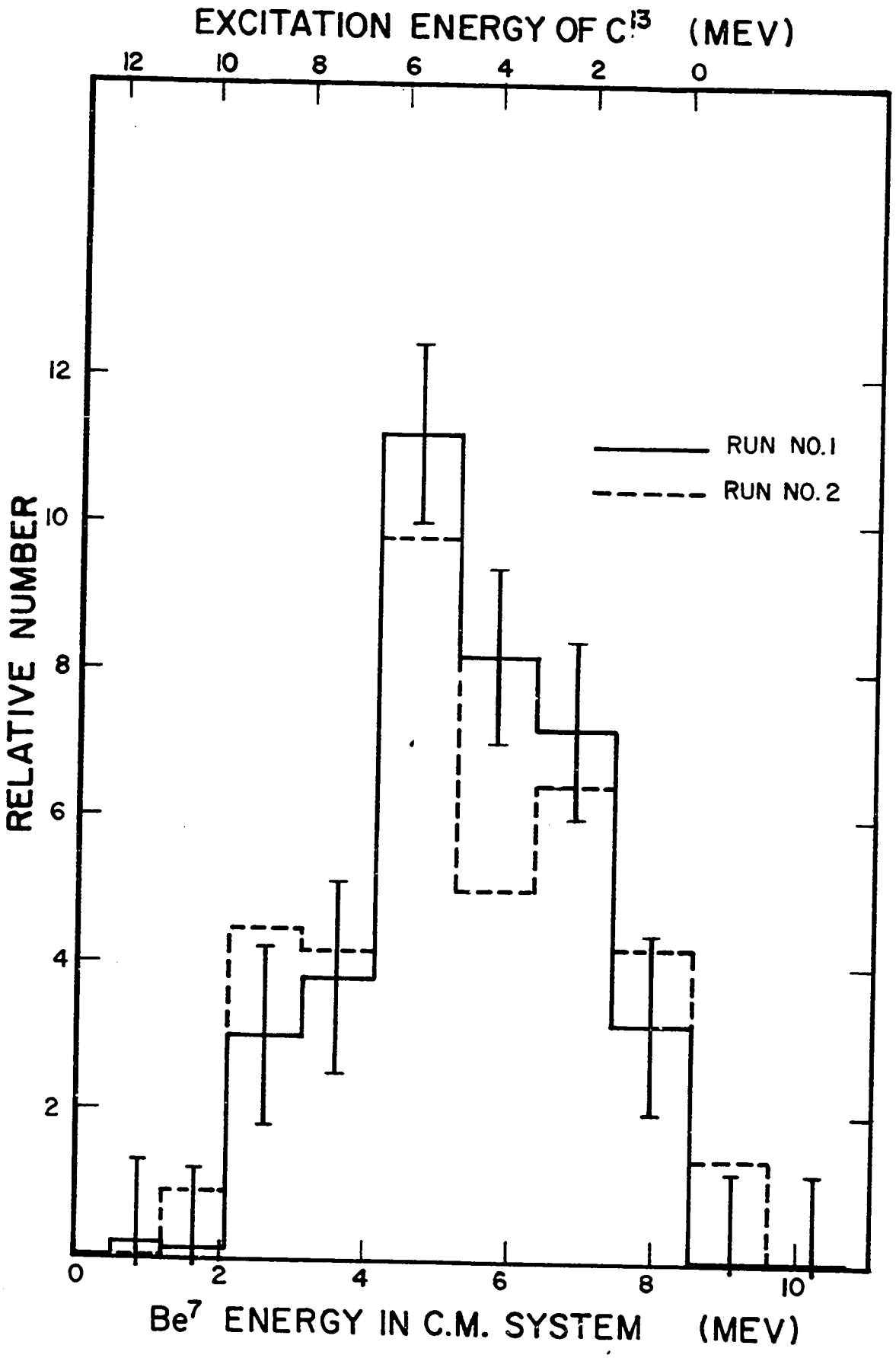
EXCITATION ENERGY OF C13 (MEV)
12
10
8
6
4
2
0
RELATIVE NUMBER
12
10
8
6
4
2
RUN NO.1
RUN NO.2
0
2
4
6
8
10
Be7 ENERGY IN C.M. SYSTEM (MEV)

and the peak of the distribution corresponds closely to the energy the Be^7 fragment must have to just go over the top of the coulomb barrier. The height of the coulomb barrier is 5.6 Mev. These observations are qualitatively in agreement with compound nucleus theory.

The smooth curve in Figure 5 is a theoretical evaporation spectrum. According to statistical theory, the probability of observing a Be^7 fragment of energy E is given by

$$dP/dE = (E - V_{eff.}) \exp. (-E/T)$$

where $T = (E/a)^{1/2}$ is the nuclear temperature, here taken as 2 Mev. A/10 was used for the parameter a. $V_{eff.}$ is the effective coulomb barrier, arbitrarily taken as 2/3 V = 3.7 Mev. The area under the curve has been normalized to the area under the histogram in the energy range 3.8 to 8.3 Mev. The fit is probably better than we have a right to expect since statistical theory may not be applicable to a nucleus as light as C^{13}. The excess Be^7 on the low energy side of the curve, down to about 3 Mev, can be accounted for by the poor resolution inherent in the experiment. Fragments with kinetic energies below about 3 Mev, in the C. M. system, are most likely contributed by large angle scattering events in the target. On the high energy side of the curve poor resoltuion works in favor of theory to produce a good fit.

An examination of Figure 3 makes it apparent that it is impossible to get angular distribution data for the backward hemisphere. Many of the Be^7 fragments would have insufficient energy to escape from the target. However, the yield in the backward hemisphere can be determined by measuring the Be^7 activity retained in the target. Table 1 shows how the total activity divides between the forward and backward hemispheres in the C. M. system. The column labeled "calculated" gives the expected total activity calculated from the measured value of the integral cross section, 3.2 millibarns, and the amount of beam to which the target was exposed. Integral cross section determinations are described in section G. The numbers are in counts per minute. The errors for the calculated values are based on an estimated 15% precision in cross section measurements.

TABLE 1

Run Number	Forward Hemisphere (C.M.)	Backward Hemisphere (C.M.)	Total	Calculated
2	[illegible] ± 15	336 ± 14	728 ± 30	805 ± 120
3	788 ± 25	760 ± 32	1548 ± 57	1120 ± 230

The expectation that the fragments could not escape from the target in the backward direction was checked by interposing thin gold foils

between the target and the beam. No appreciable amount of Be^7 activity was found in these foils.

The angular distribution in the forward hemisphere is displayed in Figure 7. The results of three runs have been superimposed to show the extent of agreement between runs. Some representative error limits are included. Each run utilized a target of different thickness: 0.6, 0.9, and 1.2 mg/cm^2 of MoO_3. Center of mass transformations are based on an assumed mean Be^7 fragment energy of 5.3 Mev in the C.M. system. This value represents the most probable energy, as is seen from Figure 5. The differential cross section apparently continues to decrease beyond 90°. This must be expected, regardless of the actual distribution in the backward hemisphere, because the Be^7 fragment finds it increasingly difficult to get out of the target at angles greater than about 100° (60° in the laboratory system). Actually, the differential cross section must rise at angles greater than 90° in order to account for the nearly equal yields in the forward and backward hemispheres.

The binding energy of a neutron in the C^{13} nucleus is only about 5 Mev. Thus if C^{13} is left with more than 5 Mev of excitation energy it may emit a neutron. If the reaction goes through a compound nucleus, the neutron could be emitted prior to the emission of Be^7

FIGURE 7

The angular distribution of Be^7 fragments from oxygen for three runs. Some representative error limits are shown. Center of mass corrections are based on a Be^7 fragment energy of 5.3 Mev in the C.M. system. Three different target thicknesses were used: 0.6, 0.9, and 1.2 mg/cm^2 of MoO_3.

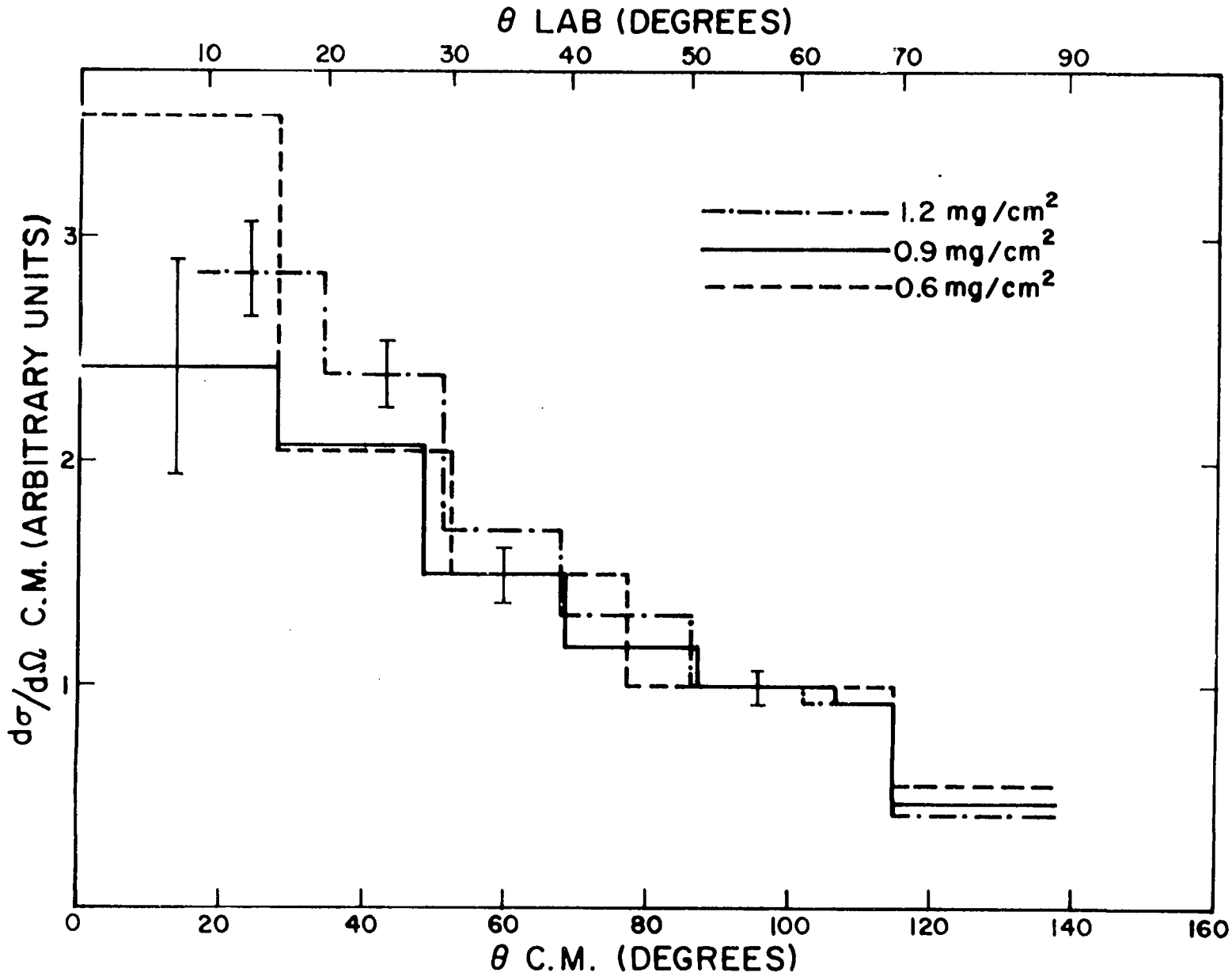
θ LAB (DEGREES)
10
20
30
40
50
60
70
90
1.2 mg/cm²
0.9 mg/cm²
0.6 mg/cm²
dσ/dΩ C.M. (ARBITRARY UNITS)
3
2
1
0
20
40
60
80
100
120
140
160
θ C.M. (DEGREES)

which would effect the energy and angular distributions of Be^7 fragments. However, this "second chance" Be^7 emission should be very improbable compared with "first chance" emission because of the drastic reduction in energy available for Be^7 evaporation. This is supported by the steepness of the excitation functions shown in Figure 16. In any case, the effect would be small and has been ignored in the treatment of the data.

B. Aluminum.

The possible energy values of Be^7 fragments from aluminum as a function of angle are given in Figure 8. The same considerations were used in establishing maximum and minimum values as those used in the corresponding figure for oxygen. The area between the two curves represents the range of possible energy values. Fortunately the decreased center of mass energy for an aluminum target makes it feasible to obtain angular distribution data in the backward hemisphere. A backward moving Be^7 fragment should have enough kinetic energy to escape from a thin target. However, scattering in the target foil may be a problem.

Figures 9 and 10 show the energy distribution data in the laboratory system. The error limits are large for all measurements made with aluminum targets because of the small cross section for the reaction

FIGURE 8

The possible energy values of Be^{7} fragments from aluminum as a function of angle. The upper curve is calculated on the basis of a 42.5 Mev incident helium ion and the Q value for the reaction Al^{27} (He^{4}, Be^{7}) Na^{24} when both products are formed in their ground states. The lower curve is calculated by assuming an effective coulomb barrier 2/3 that of the maximum coulomb barrier.

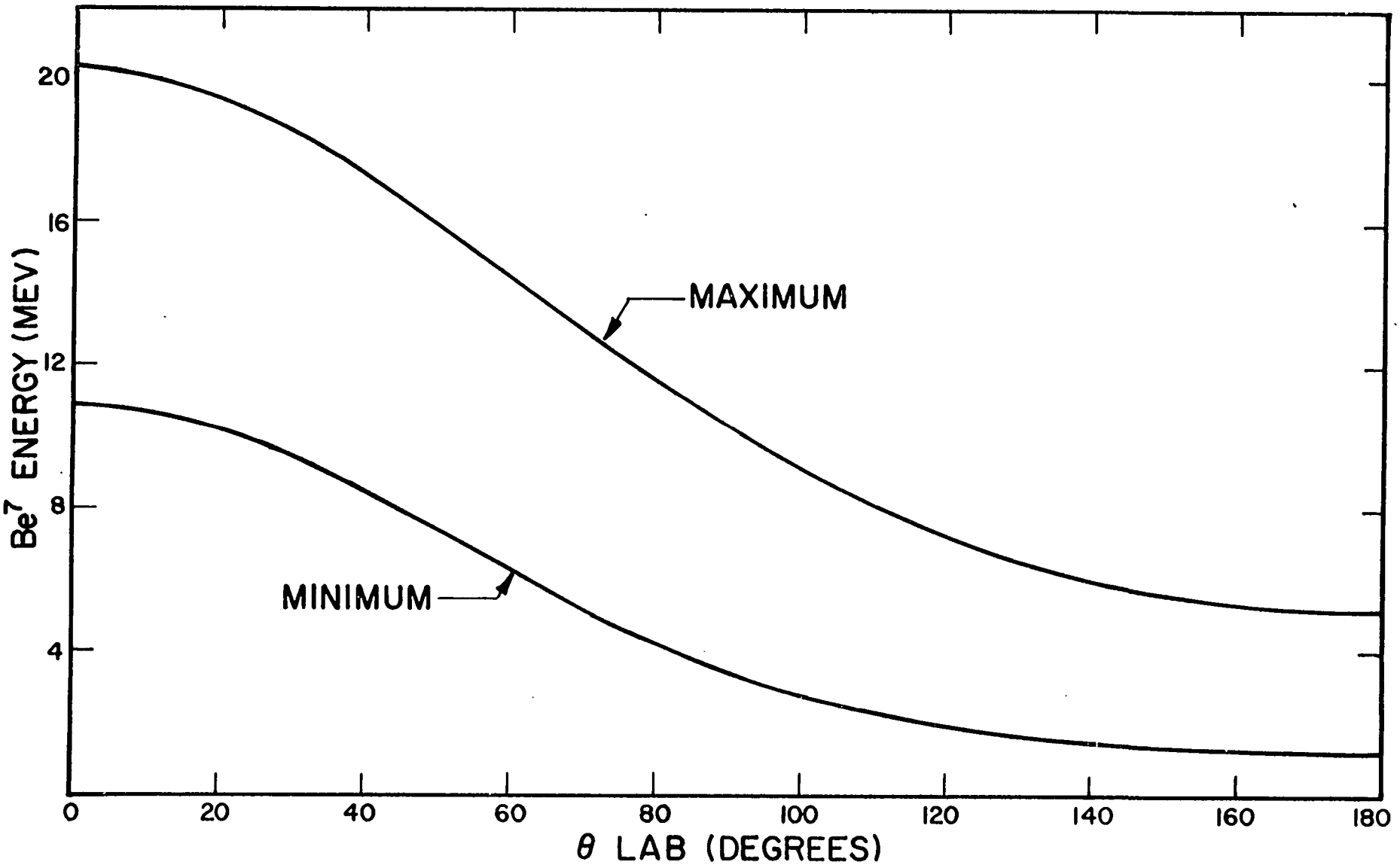
20
16
12
8
4
Be⁷ ENERGY (MEV)
MAXIMUM
MINIMUM
0
20
40
60
80
100
120
140
160
180
θ LAB (DEGREES)

FIGURE 9

The energy distribution of Be^7 fragments from aluminum in the laboratory system in the angular range 20° to 30°. Error limits derive from counting statistics, an assumed 3% error in chemical yield factors, and from the subtraction of blank-run activity. The target was 0.42 mg/cm^2 of aluminum foil.

FIGURE 10

The energy distribution of Be^7 fragments from aluminum in the laboratory system in the angular range 0° to 30°. Error limits derive from counting statistics, an assumed 3% error in chemical yield factors, and from the subtraction of blank-run activity. The target was 0.72 mg/cm^2 of aluminum foil. The vertical, hatched bars indicate the expected limits of the energy distribution as ascertained from Figure 8. The thickness of the bars indicates the extent of kinematic broadening over the angular range 0° to 30°.

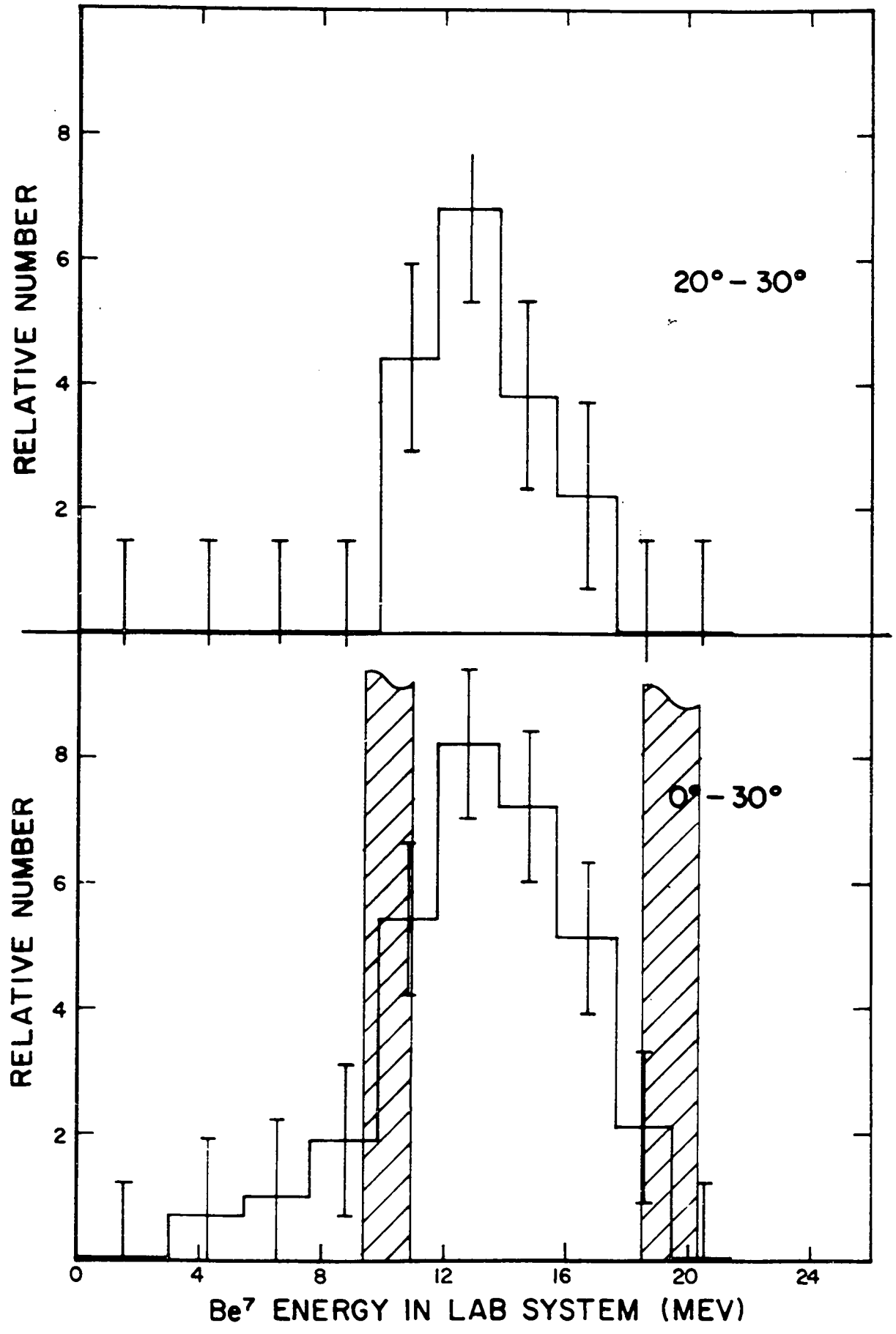
RELATIVE NUMBER
20° – 30°
RELATIVE NUMBER
0° – 30°
2
4
6
8
0
4
8
12
16
20
24
Be⁷ ENERGY IN LAB SYSTEM (MEV)

and because of spurious activity, found in blank runs, which had to be subtracted from the data. The blank runs will be described in a following section. Figure 11 shows the data of Figure 10 plotted in the C.M. system. The smooth curve is a theoretical evaporation spectrum, calculated in the same way as for oxygen, with T = 1.7 Mev and $V_{eff.}$ taken as 2/3 of the maximum coulomb barrier, or 6.1 Mev. The energy distribution is broad and the number of fragments increases with decreasing kinetic energy until the top of the coulomb barrier is reached and begins to inhibit the reaction. The data look a good deal like the results obtained for oxygen targets, except that there seems to be too many low energy fragments. However, if the effective coulomb barrier, which after all is not well known, is reduced by about 0.5 Mev the apparent low energy excess can be accounted for. Some of the low energy yield may result from large angle scattering events in the target and from an under-correction for blank run activity. The latter source of error should not exceed the error limits on the data points.

Table 2 compares the Be^7 activity found in the forward and backward hemispheres. The numbers are in counts per minute. The column headed "calculated" lists the expected total activity for each run based on an integral cross section of 0.314 millibarns (see

FIGURE 11

The energy distribution of Be^7 fragments from aluminum in the C.M. system in the angular range 0° to 30°. The data is the same as that of Figure 10. The abscissa at the top of the figure gives the excitation energy left in the product nuclei for any given Be^7 energy. Since the highest reported bound state of Be^7 is at 0.43 Mev, this may be regarded as the excitation energy left in the Na^{24} nucleus. The smooth curve is a fit to

$$\frac{dP}{dE} = (E - V_{eff.}) \exp\left(-\frac{E}{T}\right) .$$

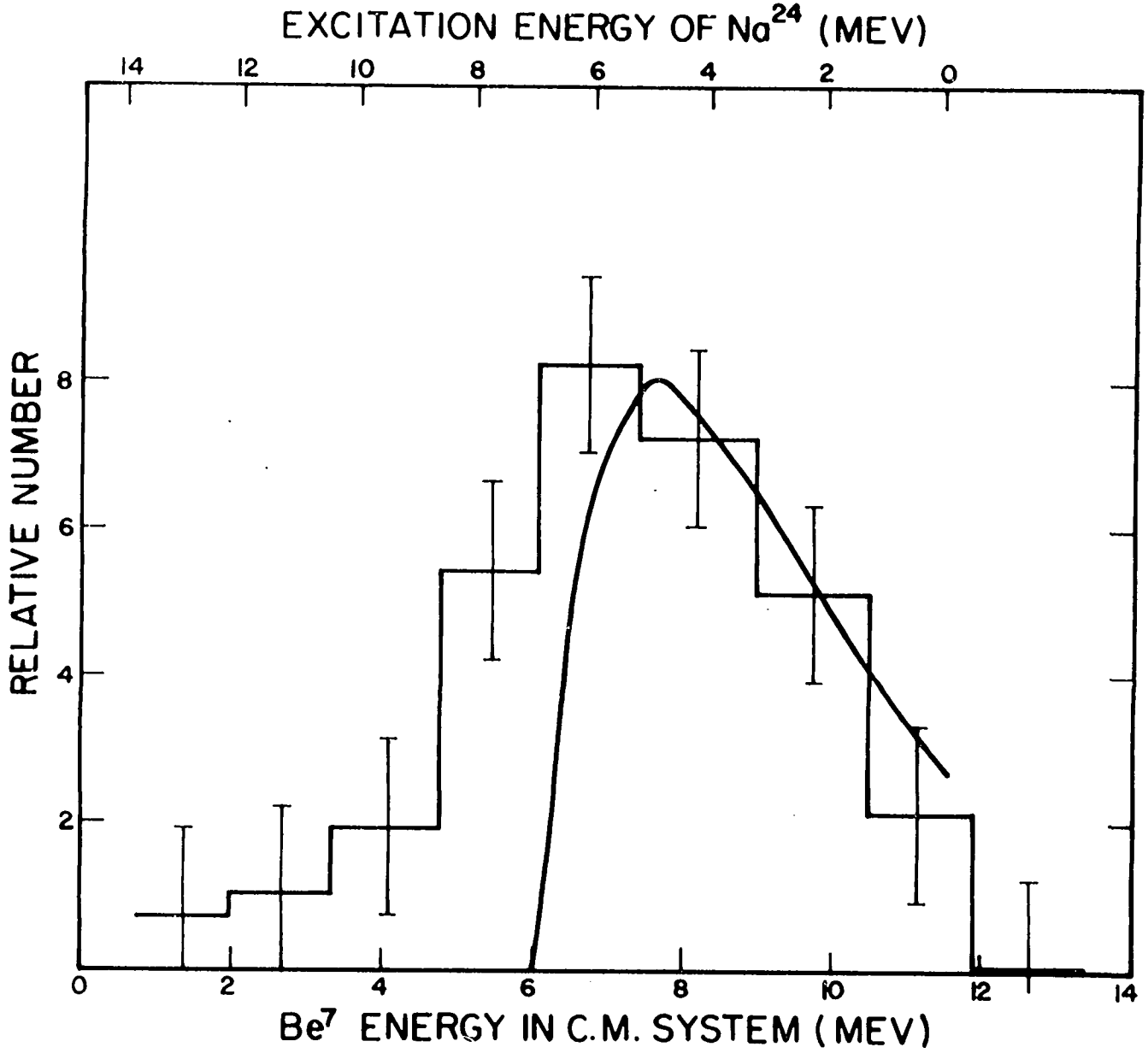
EXCITATION ENERGY OF Na^{24} (MEV)
14
12
10
8
6
4
2
0
RELATIVE NUMBER
8
6
4
2
0
2
4
6
8
10
12
14
Be^7 ENERGY IN C.M. SYSTEM (MEV)

Section G). The errors for the calculated values are based on an estimated 15% precision in cross section measurements. Errors for yields in the forward hemisphere are larger because the correction for blank-run activity was largest at forward angles. The error limits for run number 1 are smaller than for runs 2 and 3 because the target was thicker and blank-run activity was a smaller fraction of the total activity.

TABLE 2

Run Number	Forward Hemisphere (C.M.)	Backward Hemisphere (C.M.)	Total	Calculated
1	109.6 ± 21	69.1 ± 7	179 ± 28	163 ± 24
2	112.2 ± 47	70.1 ± 10	182 ± 57	208 ± 31
3	90.7 ± 22	48.3 ± 8.5	139 ± 30	98 ± 15

There appears to be 60% to 80% more activity in the forward hemisphere than in the backward hemisphere, although the large error limits make this conclusion somewhat uncertain. Moreover, most of the uncertainty in the numbers is not statistical in nature so the fact that all three runs give about the same results does not strengthen the conclusion. If the numbers are taken at face value they indicate that direct interactions contribute substantially to the total cross section. In any case, because of the large yield in the backward hemisphere, it is likely that the reaction frequently goes through a compound

nucleus.

The angular distribution data from run number 3 are presented in Figure 12. Center of mass corrections are based on a Be^7 fragment energy in the C.M. system of 6.9 Mev, taken to be the most probable energy. The target was 0.42 mg/cm^2 of aluminum foil. The data from run number 2 are similar in every respect except that the error limits are larger. Run number 1 was not designed to give angular distribution data.

The distribution at backward angles is probably distorted to some extent by scattering in the target foil. The effect should be to make the angular distribution in the backward hemisphere appear flatter than it really is. This conspires with the large error limits at forward angles to make the true shape a bit obscure. It can be said, however, that the angular distribution for Be^7 fragments from aluminum is approximately symmetric about 90° and peaks at 0° and 180°. Qualitatively, the data are in agreement with compound nucleus theory.

There is just enough energy available to the compound nucleus, P^{31}, for it to eject both a neutron and a Be^7 fragment. If Na^{24} is left with more than about 7 Mev of excitation energy it may evaporate a neutron. An examination of Figure 11 shows that the Be^7 fragment almost always will carry away so much energy that not enough

FIGURE 12

The angular distribution of Be^7 fragments from aluminum. Error limits derive from counting statistics, an assumed 3% error in chemical yield factors, and from the subtraction of blank-run activity. Center of mass corrections are based on a Be^7 fragment energy of 6.9 Mev in the C.M. system. The target was 0.42 mg/cm^2 of aluminum foil.

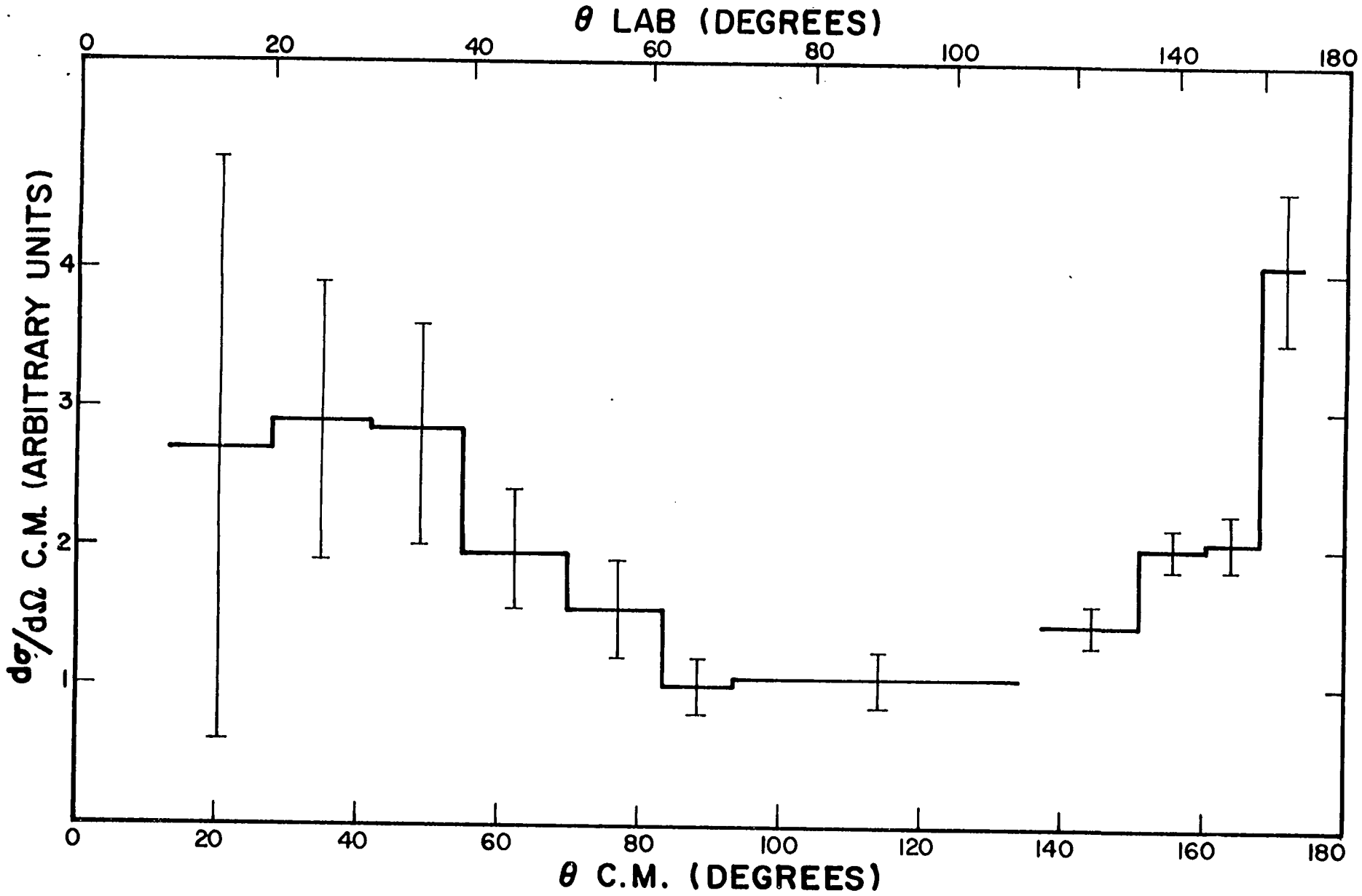
θ LAB (DEGREES)
0
20
40
60
80
100
140
180
dσ/dΩ C.M. (ARBITRARY UNITS)
1
2
3
4
0
20
40
60
80
100
120
140
160
180
θ C.M. (DEGREES)

excitation energy is left behind for neutron evaporation. We are justified, therefore, in thinking of Be^7 production from aluminum in terms of the reaction Al^{27} (He^4, Be^7) Na^{24}.

C. Carbon.

In the helium ion bombardment of carbon, Be^7 can be produced in two different ways. It can result directly from the reaction C^{12} (He^4, Be^7) Be^9, the reaction of interest here, or it can be left as a residue of the spallation reaction C^{12} (He^4, $2\alpha n$) Be^7. If Be^7 is left as a residue it should have a broad energy distribution, peaked around the average momentum of the Be^7 fragment in the C.M. system. It is estimated that this peak would be at about 8.5 Mev in the laboratory system. If Be^7 is produced by the first reaction it should have an energy distribution with the upper limit fixed by the ground state Q value of the reaction and a lower limit fixed by the coulomb barrier. This gives an energy range at zero degrees of about 11.5 Mev to 17.3 Mev in the laboratory system, when the effective coulomb barrier is taken as 2/3 V = 2.7 Mev.

Figure 13 shows the energy distribution of Be^7 fragments from carbon in the angular range 0° to 10°. It is seen to be very broad with a distinct suggestion of two peaks. The positions of the two peaks are in keeping with the idea that both reactions are contributing

FIGURE 13

The energy distribution of Be^{7} fragments from carbon in the angular range 0° to 10°. The error limits derive from counting statistics. The target thickness was 0.7 mg/cm^{2}.

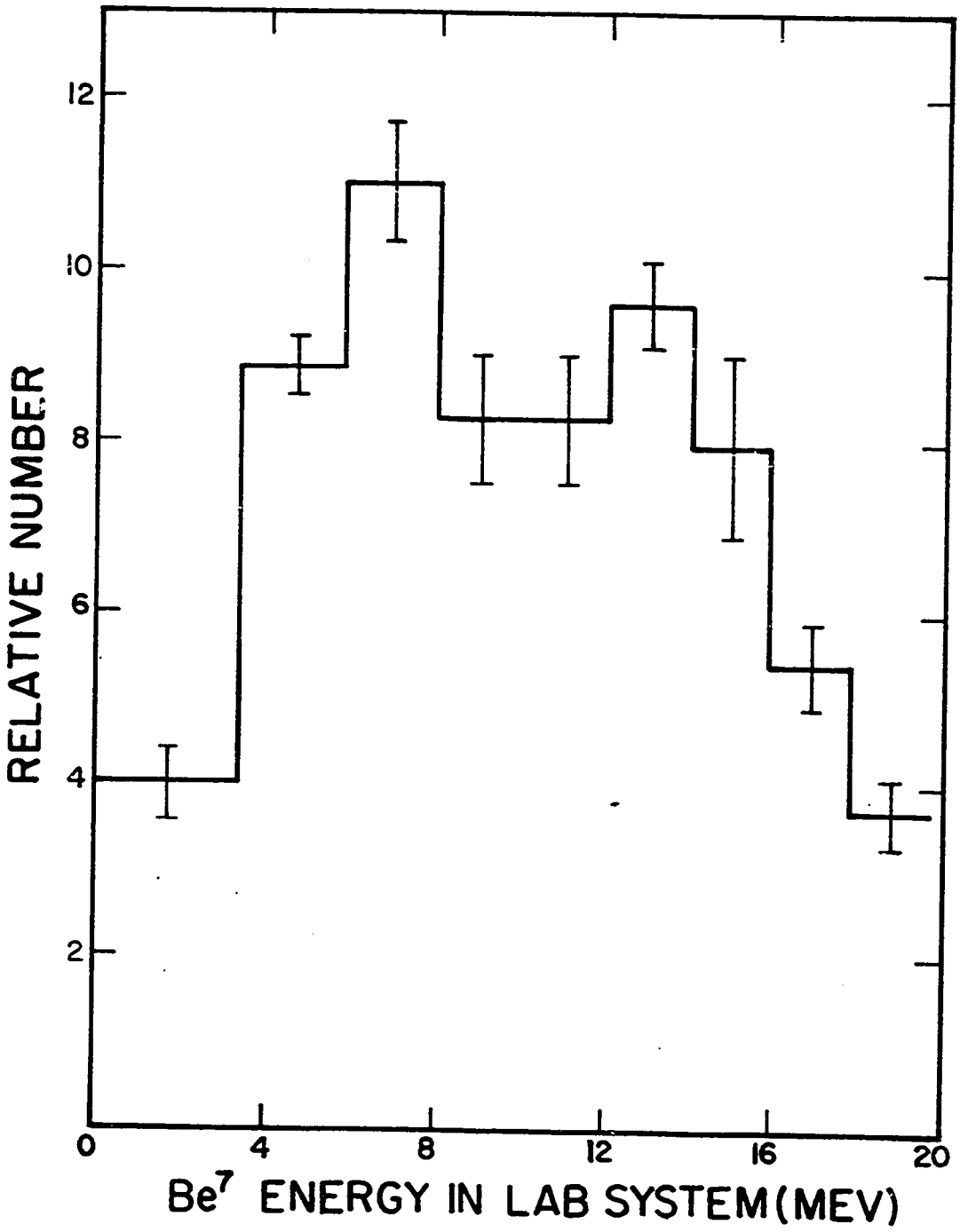
RELATIVE NUMBER
0
2
4
6
8
10
12
0
4
8
12
16
20
Be⁷ ENERGY IN LAB SYSTEM (MEV)

to the Be^7 cross section.

An attempt was made in the angular distribution experiment to distinguish between the two reactions by catching the Be^7 fragments in a stack of gold foils. The stack was divided into two parts corresponding to Be^7 energies of 0 Mev to 10 Mev and 10 Mev to 19 Mev. The results are shown in Figure 14. It is seen that the energetic fragments have a somewhat steeper angular distribution, but this would be expected for either of the postulated reactions.

The fact that two different reactions probably contribute to the Be^7 cross section for carbon makes the interpretation of the data uncertain. For this reason no further work was done with carbon targets. For target elements heavier than nitrogen it is energetically impossible to obtain Be^7 as a spallation residue, with the available beam energy, and this confusion is eliminated.

Neither the angular distribution nor the energy distribution data reproduce the salient results of the counter experiment of Nicholson and Hower (described in Appendix II and reference (26-18). They observed two peaks in the energy spectra of Be^7 fragments from carbon which were associated with transitions to the ground state and first excited state of Be^9 in the reaction C^{12} (He^4, Be^7) Be^9. The ground state transition predominated and fell off rapidly with angle from 5° to 20°. Observations at larger angles and lower fragment

FIGURE 14

The angular distributions of Be^7 fragments from carbon in the laboratory system. The solid line is for low energy fragments in the range 0 to 10 Mev. The dashed line is for high energy fragments in the range 10 to 19 Mev. Errors are of the order of 10%. The target thickness was 2 mg/cm^2.

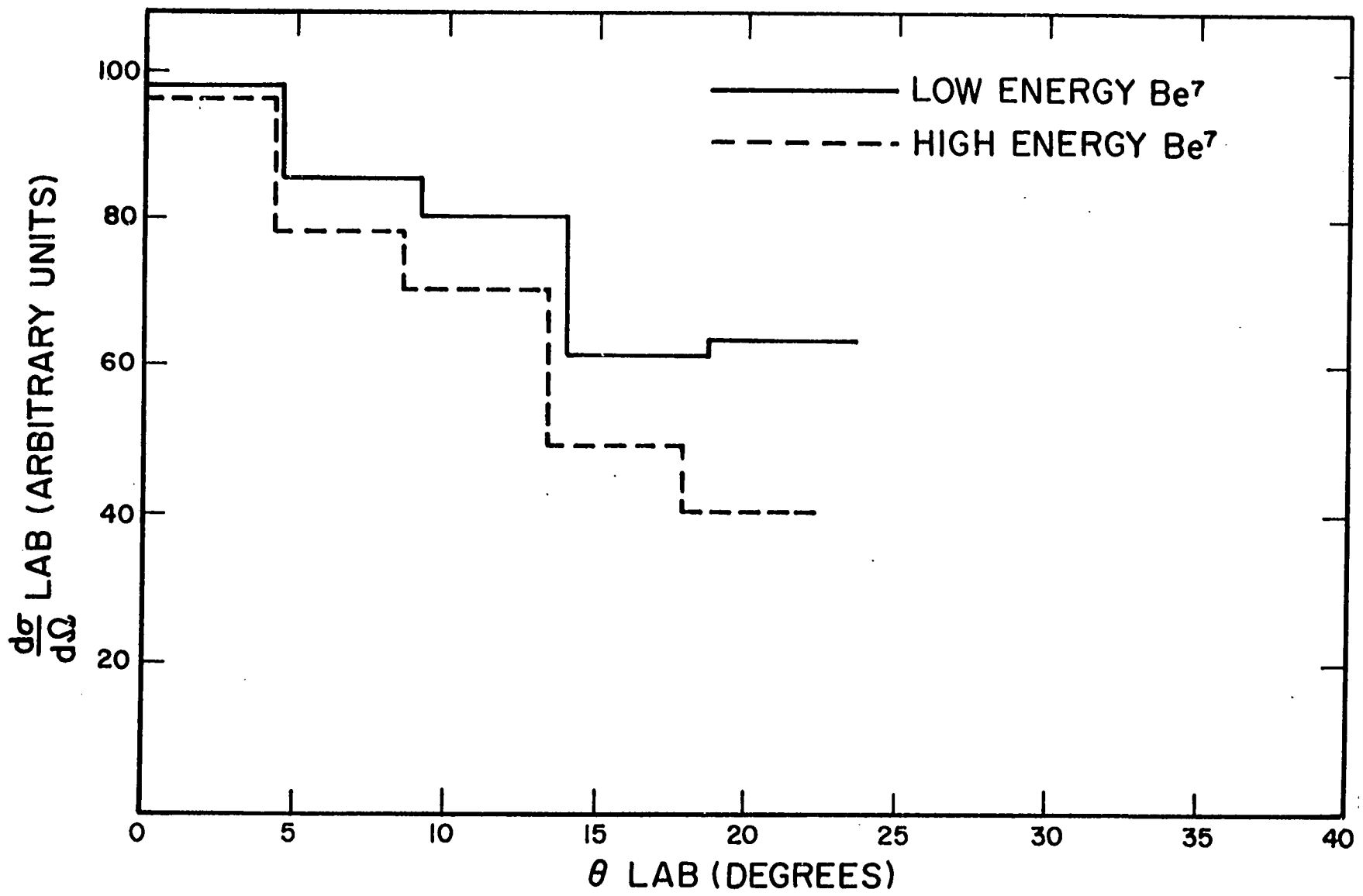
LOW ENERGY Be7
HIGH ENERGY Be7
dσ/dΩ LAB (ARBITRARY UNITS)
θ LAB (DEGREES)
100
80
60
40
20
0
5
10
15
20
25
30
35
40

energies were precluded by the high threshold energy of the counter. These results may indicate a direct interaction contribution, which the chemical experiments do not see because of the overwhelming number of low energy fragments.

D. Scattering.

As Be^7 fragments emerge from a target foil some of them will be scattered by collisions with target nuclei. Obviously this will have a distorting effect on angular distribution data. The purpose of this section is to show that scattering is not a serious concern for the measurements just described.

The problem will be considered in two parts. First is the scattering of Be^7 fragments which come out of the target at angles less than about 70° or greater than about 110°. That is, we first consider only those fragments which see a thin target. At 3 Mev of kinetic energy and above, the Be^7 fragment should be fully ionized if we make the assumption that it will not start to capture electrons until its linear velocity is less than the orbital velocity of an inner Be electron. Thus the well-known Rutherford scattering equation can be applied with some confidence. The outline of Bethe and Ashkin (4-248) is followed here. If the mass of the Be^7 ion is considered to be small compared with the masses of the target nuclei, then the differential cross section

for scattering into the solid angle $2\pi \sin\theta \, d\theta$ is

$$d\sigma(\theta) = \frac{2\pi e^4 z^2 Z^2}{16 E^2 \sin^4 \frac{\theta}{2}} \sin\theta \, d\theta$$

where z and Z are the atomic numbers of Be and the target element respectively and E is the energy of the Be^7 fragment. Integrating over the angles θ to π and multiplying by the number of target nuclei per cubic centimeter, N, gives the total number of scattering events per centimeter of target into an angle greater than θ:

$$N \int_{\theta}^{\pi} d\sigma(\theta) = \frac{\pi e^4 z^2 Z^2 N}{4E^2} \cot^2 \frac{\theta}{2}$$

For a 0.5 mg/cm^2 aluminum target this reduces to:

$$\text{No. scattering events into an angle} > \theta = \frac{4.9 \times 10^{-4}}{E(\text{Mev})^2} \cot^2 \frac{\theta}{2}$$

As an example, for E = 3 Mev, one Be^7 fragment out of 35 will be scattered through an angle greater than 5°. However, the probability for scattering increases rapidly as the scattering angle decreases and the cumulative effect of successive small angle scattering events must also be examined. Expressions for the average scattering angle experienced by charged particles in traversing a thin foil are well known. Using the equation given by Bethe and Ashkin (4-285) it can be shown that the multiple scattering of energetic Be^7 fragments in a

thin target is a small effect. A 3 Mev Be^7 fragment traversing 1 mg/cm^2 of aluminum will on the average be scattered through an angle of about 2.5°. A 10 Mev fragment would suffer an average deflection of about 1°. Hence, the scattering of energetic fragments is not a problem as long as the target is thin. A look at Figure 8 shows that some Be^7 fragments emitted in the backward direction from aluminum may have only 1.5 Mev of kinetic energy. The Rutherford equation is not valid for such low energies and it is difficult to make a good estimate of the scattering cross section for these fragments. However, it is not likely that these low energy events would have a large effect on the angular distribution because there are relatively few fragments with energies this low.

The target will not be thin to those fragments which come out at angles near 90°; it will be thick and large angle scattering should be highly probable. Fortunately there are not many such fragments compared with the total cross section. Some idea of the frequency of these large angle scattering events can be obtained by examining the data. Be^7 emitted at angles near 90° and scattered into small angles must show up in the energy distributions as low energy fragments. As an example, consider the energy distribution of Be^7 fragments from oxygen in Figure 4. If it is assumed that all of the

fragments below 8 Mev result from scattering, then scattering contributes about 10% of the yield in the angular range 20° to 30°. This is probably an overestimate as some of the low energy yield must be due to straggling. Although 10% is a significant amount, it is not a particularly damaging amount. Another indication that scattering has no large effect is the fact that the angular distributions for oxygen show little or no dependence on target thickness, even though the thickness of the targets was varied by a factor of 2.

In conclusion, scattering should not be a source of any anxiety, with the possible exception of the angular distribution for aluminum in the backward hemisphere.

E. Blank Runs.

Because of the very low counting rates encountered in these experiments, it was essential to make sure that all the Be^7 activity measured actually originated in the target. For this reason several blank runs were made wherein a thin gold foil was substituted for the target. The catcher foils were then processed in the usual manner and counted. Unhappily, spurious Be^7 activity was observed. It was always confined to the forward hemisphere, none was found in the backward hemisphere. It is believed that the deposition of pump oils on the target foil during the long bombardments (up to 40 hours) was responsible.

The cross section for Be^7 production from helium ions on carbon is large, about 4 millibarns, and the center of mass energy would throw the entire yield into the forward hemisphere. Blank run activity was subtracted out of all the data. For oxygen the correction was small but for the aluminum data the correction was severe, as large as 75% in some instances.

F. Oxygen Content of Aluminum Targets.

Since the cross section for the oxygen reaction is about ten times that of the aluminum reaction it was necessary to prove that the oxygen content of the aluminum target foils was within tolerable limits. If the oxide film on the aluminum targets were very thick it could seriously distort the aluminum data. The thickness of the oxide film was measured by activation analysis. Aluminum target foils were exposed to the helium ion beam and the resulting F^{18} was counted with a well crystal and single channel analyzer.

Calibration was accomplished by building up the Al_2O_3 film on aluminum foil to a known thickness. This was done by anodizing ordinary Reynold's Wrap in a hot saturated solution of boric acid at 300 volts. The thickness of the oxide film was determined by weighing large areas of the anodized foil. The foils were placed in the helium ion beam for about 5 minutes and then counted. The decay curves were corrected for a 15 hour Na^{24} tail, although the 1.87 hour F^{18}

activity was very prominent. The results are plotted in Figure 15. This proved to be an extremely sensitive test for oxygen. It is estimated that with an accurate calibration, less than microgram quantities of oxygen could be easily determined. Of course, the F^{18} would have to be chemically purified before counting if other activities with similar half lives were produced at the same time.

The oxygen content of aluminum targets was measured both before and after a bombardment. Before a bombardment the oxygen content was 1.5^{+2}_{-1} $\mu g/cm^2$. After a bombardment it was $3.5^{+2.5}_{-1.5}$ $\mu g/cm^2$. The results agree well with values reported in the literature (7-13) for Al_2O_3 films formed at room temperatures. The aluminum data were corrected for the oxygen contamination of the targets. This correction was very small except for the target foil itself, where it was about 20%, because the low laboratory energy of backward-directed fragments from oxygen did not permit them to escape the target.

G. Cross Section Measurements.

Table 3 lists the cross section data for Be^7 production obtained from the helium ion bombardment of carbon, nitrogen, oxygen, fluorine and neon. No systematic investigation of the various sources of error was undertaken so error limits are not included. Reasonable care was taken with the measurements, however, and the reported absolute

FIGURE 15

Fluorine-18 activity as a function of the oxygen content of aluminum foil.

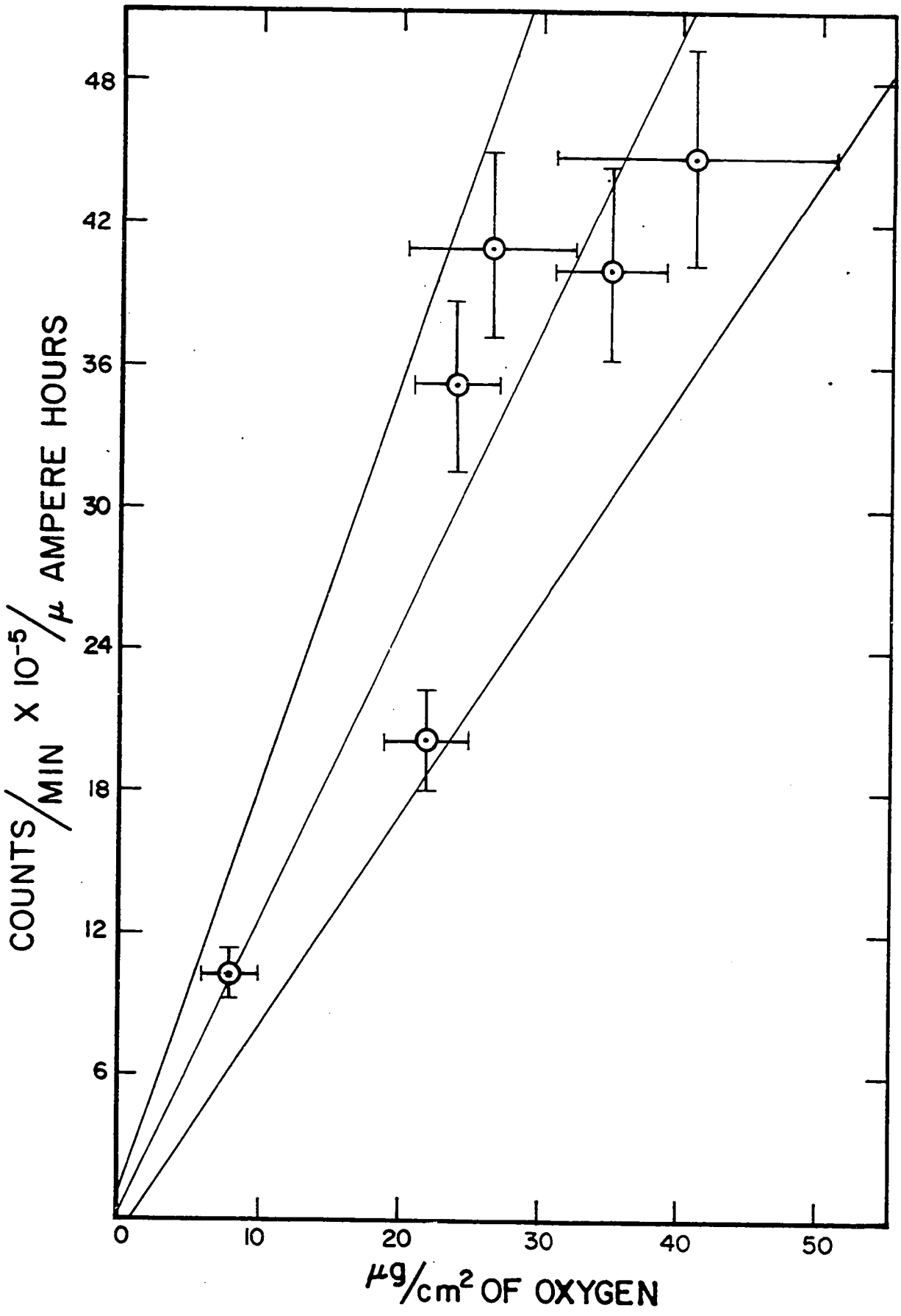
48
42
36
30
24
18
12
6
0
10
20
30
40
50
COUNTS/MIN X 10⁻⁵/μ AMPERE HOURS
μg/cm² OF OXYGEN

TABLE 3

Cross Sections for Be^7 Production from Helium Ion Bombardment of Several Light Elements.

Target Element	Disintegration Rate, counts/sec.	μampere hours of beam	Target thickness, mg/cm^2	Ave. beam energy, Mev	Cross section, cm^2
Carbon	27800	38.2	2.39	42.2	3.55×10^{-27}
	12500	28.2	1.53	41.2	3.38×10^{-27}
	5920	28.2	2.05	38.8	1.2×10^{-27}
	3920	38.2	2.54	37.9	4.7×10^{-28}
	1180	21.1	5.55	37.7	1.17×10^{-28}
	< 56	21.1	1.85	35.0	$< 1.7 \times 10^{-29}$
	< 33	38.2	2.65	33.2	$< 3.8 \times 10^{-30}$
Nitrogen	3760	24.0	1.15	38.1	1.85×10^{-27}
	6780	23.0	2.16	38.0	1.85×10^{-27}
	2400	24.0	1.15	35.7	1.18×10^{-27}
	4150	23.0	2.16	35.4	1.13×10^{-27}
	2040	24.0	2.30	32.9	5.0×10^{-28}
	582	23.0	2.16	31.2	1.58×10^{-28}
	409	24.0	2.30	30.8	1.0×10^{-28}
Oxygen	1420	3.64	1.9	41.7	3.2×10^{-27}
	625	3.64	1.9	37.6	1.4×10^{-27}
	159	3.64	2.26	33.2	3.0×10^{-28}
	< 2	3.64	2.26	30.5	$< 4 \times 10^{-30}$
Fluorine	1190	4.68	1.88	41.8	2.5×10^{-27}
	351	4.68	1.88	38.2	7.35×10^{-28}
	106	4.68	2.73	33.9	1.53×10^{-28}
	<14	4.68	2.76	31.1	$< 2.0 \times 10^{-29}$
Neon	2150	25.0	1.04	38.1	1.57×10^{-27}
	1360	25.0	1.04	35.1	9.9×10^{-28}
	955	25.0	1.04	33.8	7.0×10^{-28}
	895	25.0	1.04	32.6	6.5×10^{-28}
	760	25.0	2.08	30.0	2.8×10^{-28}
	154	25.0	2.08	29.5	5.7×10^{-29}
Aluminum	359	5.8	5.13	41.5	8.14×10^{-28}

values should be accurate to ± 20%. The error in one cross section relative to another should be less.

In Figure 16 the cross sections are plotted as a function of incident beam energy. The data for magnesium and aluminum are from Lindsay (22-2168). We note that, with the exception of carbon, these curves all have similar shapes. The high energy portion of the curves are nearly parallel, which suggests that the same mechanism is responsible for all of these reactions. As the bombarding energy is decreased the excitation functions begin to fall precipitiously. The energy at which each curve steepens is approximately equal to the threshold energy plus the coulomb barrier, indicating that barrier penetration governs the shape of the steep portion of each curve. Carbon seems to have anomalously high cross sections in view of the high threshold energy, which is a further indication that Be^7 is left as a spallation product in this case.

H. Sodium-24 Experiments

The reaction Al^{27} (He^4, Be^7) Na^{24} has been studied by measuring the range distribution and angular distribution of the Be^7 fragments. This method suffers from the low counting rates obtained for the long-lived Be^7. An alternative approach is to look at the Na^{24} residual

FIGURE 16

Excitation functions for Be^{7} production from helium ions incident on:

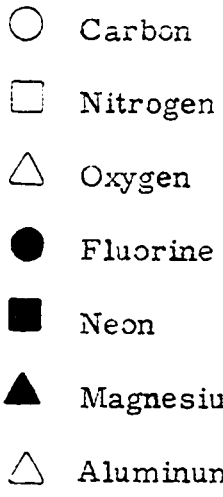

The magnesium and aluminum points are from Lindsay (22-2168).

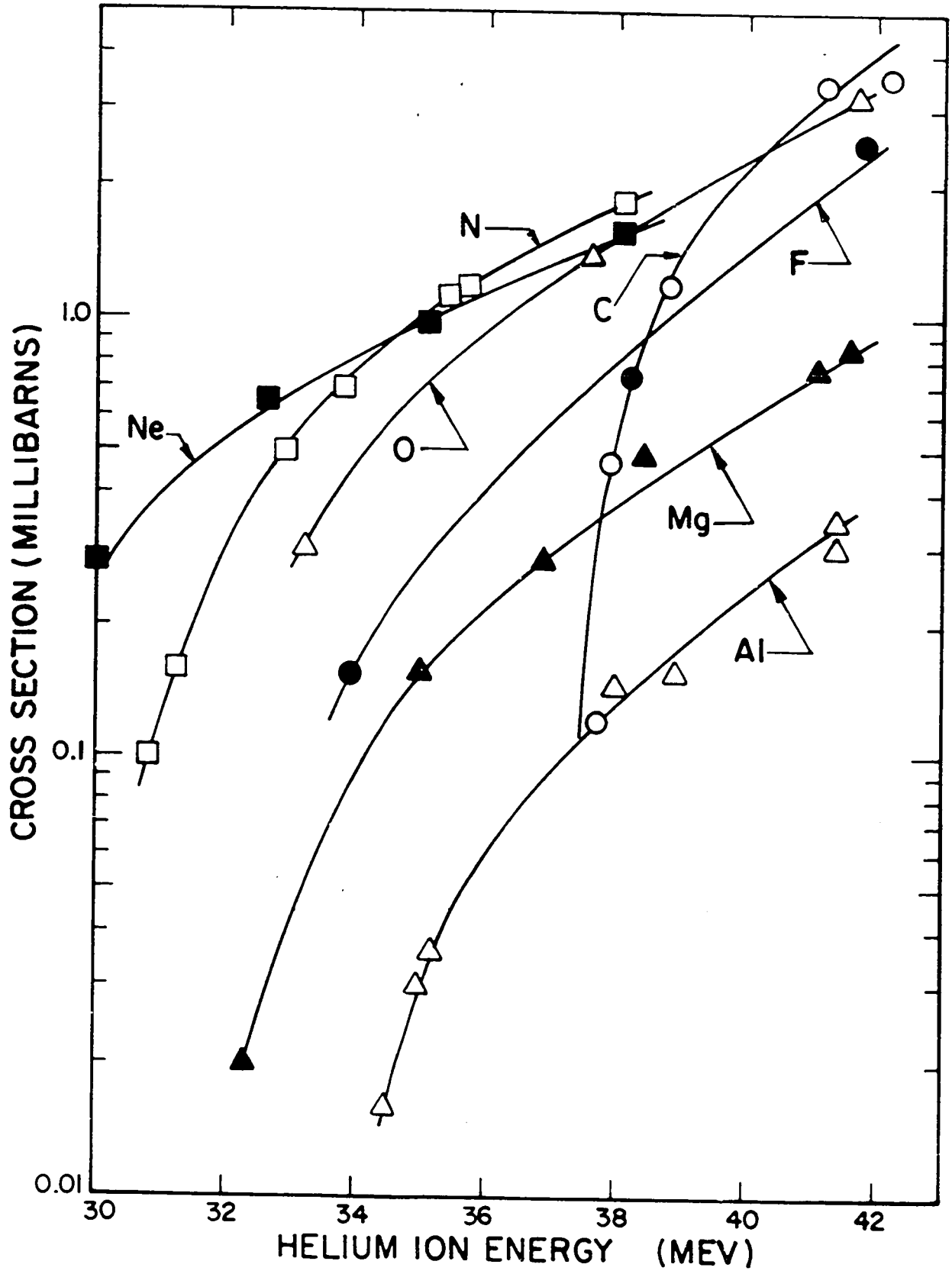
CROSS SECTION (MILLIBARNS)
1.0
0.1
0.01
30
32
34
36
38
40
42
HELIUM ION ENERGY (MEV)
Ne
N
O
C
F
Mg
Al

nucleus. A Be^7 fragment emitted into the backward hemisphere results in a forward moving Na^{24} ion with as much as 15 Mev of kinetic energy. This offers the hope of studying the backward angular distribution of Be^7 fragments by measuring the angular distribution of the forward moving Na^{24} residuals. Moreover, 4π counting of the Na^{24} beta particle,and the shorter half-life of Na^{24}, afford an increase in sensitivity over Be^7 counting by a factor of almost 10^4. This would make possible the use of very thin targets in order to obviate the scattering problem, and at no sacrifice to counting statistics. For these reasons a series of experiments was undertaken with the object of determining the angular distribution of the Na^{24} recoils. Three kinds of measurements were made: total cross sections for Na^{24} production at 42 Mev, range distributions, and angular distributions.

The same general experimental set-up diagrammed in Figures 1 and 2 was used All aluminum structural pieces were sprayed with Krylon plastic to prevent the possible collection of stray Na^{24} from the Al^{27} (n, α) Na^{24} reaction resulting from secondary neutrons. For the range experiments the recoils were caught in stacks of gold leaf foils, each foil being approximately 0.17 mg/cm^2 thick. Na^{24} was separated by standard chemical techniques (6-160), (29-21) and counted as NaCl in 4π, gas flow geiger counters.

A measurement of the integral cross section for Na^{24} production at 42 Mev gave a value of 0.57 millibarns, larger than the Be^{7} cross section by a factor of 1.8. Lindsay (22-2168) reports similar results, the Na^{24} cross section being larger by a factor of 1.5 at a bombarding energy of 41 Mev. Obviously the Be^{7} and Na^{24} approaches are not equivalent if Na^{24} is contributed by reactions which do not produce Be^{7}, as these cross section comparisons would seem to indicate. The possibility of interference from the (n, α) reaction was examined by making a run similar to the total cross section run, except that the beam was blocked off just in front of the target, allowing only neutrons to get through The total beam incident on the water arm was monitored to provide a rough means of comparing the exposure with other runs. Very little Na^{24} was found and it was determined that the (n, α) contribution to the Na^{24} cross section was less than 5%, an amount which is subsequently ignored. Apparently the neutron flux at the target position was not excessive.

The simplest explanation for the excess Na^{24} is that it is produced by the Al^{27} (He^{4}, α He^{3}) Na^{24} reaction. Such processes as (He^{4}, α 2pn) can be eliminated because their thresholds are too high. However, there is still another possibility. If about half of the Be^{7} fragments were formed in unbound excited states, they would subsequently decay

by particle emission and therefore remain undetected, thus accounting for the disparity between the observed Na^{24} and Be^{7} cross sections. The difficulty with this explanation is that the first unbound excited state of Be^{7} is at 4.5 Mev above the ground state. If for the moment we assume a compound nucleus mechanism, there is only about 14.8 Mev available for Be^{7} emission from the compound nucleus, P^{31}. This disregards an effective coulomb barrier of about 6 Mev. A further reduction of this energy by the 4.5 Mev necessary for Be^{7*} (4.5 Mev) evaporation would seem to make this event much less probable than the emission of Be^{7} in its ground state. If it is assumed that the ratio of (He^{4}, Be^{7}) to (He^{4}, Be^{7*}) is equal to the number of levels available in the residual nucleus, Na^{24}, and we use exp $2(aE)^{1/2}$ with $a = A/10$ for the level densities, we obtain a ratio of about 9:1. This value has been corrected for the 1:2 statistical weight factor between Be^{7} and Be^{7*} (4.5 Mev) due to spins.

A similar calculation gives a ratio of 1:1 for the ratio of (He^{4}, Be^{7}) to (He^{4}, $\alpha\, He^{3}$) events, assuming all particles to be emitted in their ground states. Thus the (He^{4}, $\alpha\, He^{3}$) process would seem to be favored over (He^{4}, Be^{7*}), but these estimates are much too crude to permit a choice between the two possibilities.

It was thought at first that a contribution to the Na^{24} yield from the (He^{4}, $\alpha\, He^{3}$) reaction could be detected by studying the ranges of the

Na^{24} recoils. This proved to be an overly optimistic idea. The energy distribution of the Na^{24} recoils from the (He^4, α He^3) reaction can be readily calculated if the following assumptions are made: the α and He^3 particles are uncorrelated; they have isotropic angular distributions; and they are evaporated from a compound nucleus with constant energy of about 5 Mev. The assumption of a constant energy is really quite good because there is not much energy available to the particles in addition to the energy they must have for overcoming coulomb barriers. The results of such a computation are shown in Figure 21. The curve has been rounded somewhat out of consideration for the fact that the energies of the evaporated particles are not really constant. The curve labelled "(He^4, Be^7)" is the expected energy distribution of Na^{24} recoils from the reaction of interest, based on the known energy distribution of Be^7 fragments. Both curves are estimated within the limiting laboratory angular range of 0° to 20° to correspond with the angular aperture in the experiment. The histogram gives the measured energy distribution. The experimental range distribution data were transformed into an energy distribution by using the range-energy curves of Northcliffe (28-1744) for sodium ions in aluminum and correcting for ranges in gold by the method of Hubbard (18-1). This is an uncertain procedure and for this reason the experimental energy

FIGURE 17

The experimental energy distribution of Na^{24} recoils in the angular range 0° to 20°. The curve labelled "(He^4, Be^7)" is the estimated energy distribution of recoils from this reaction. The curve labelled "(He^4, α He^3)" is the expected energy distribution from the Al^{27} (He^4, α He^3) Na^{24} reaction. Details of the calculation are given in the text.

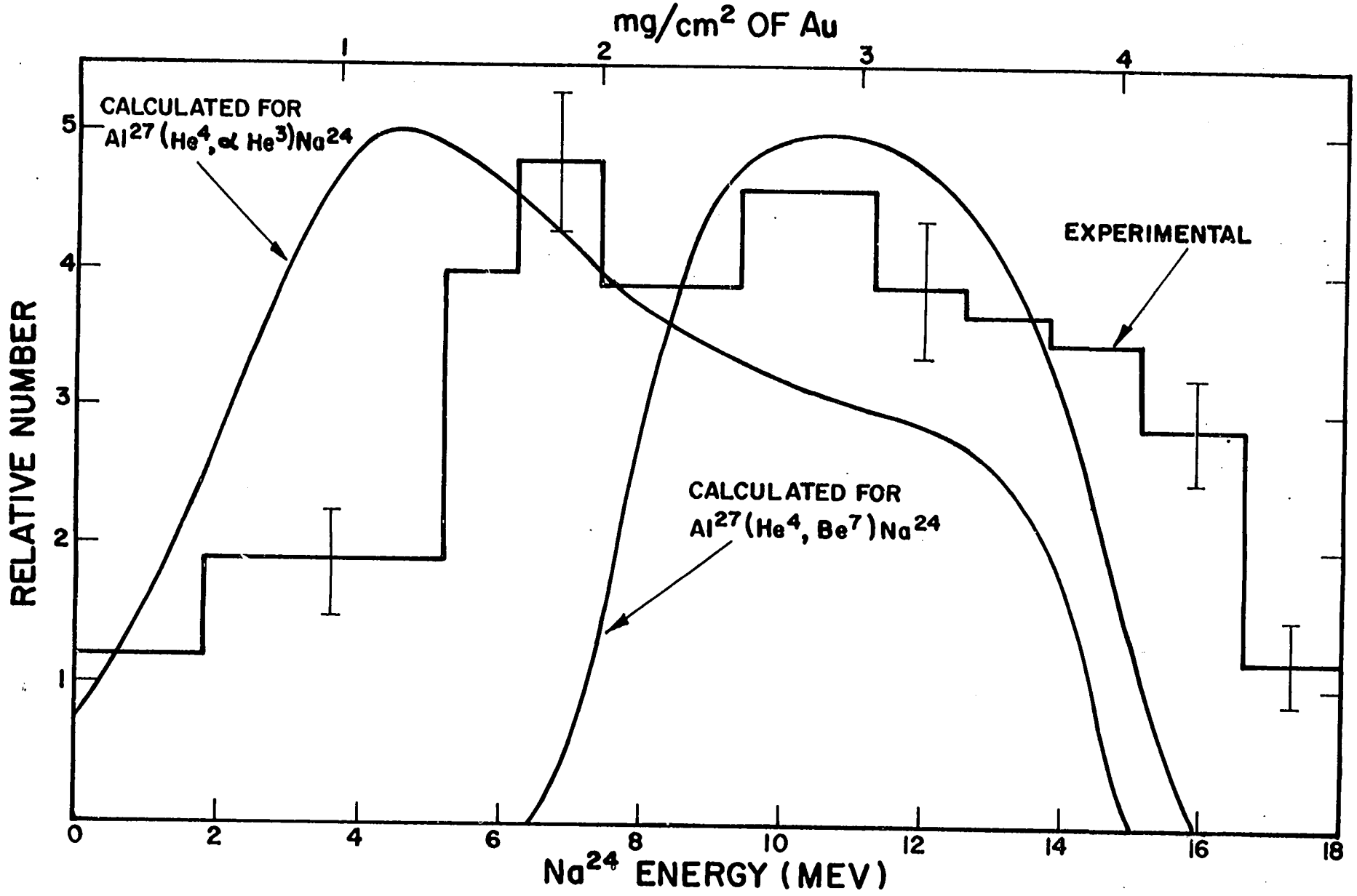
mg/cm² OF Au
1
2
3
4
CALCULATED FOR
Al²⁷(He⁴, α He³)Na²⁴
EXPERIMENTAL
CALCULATED FOR
Al²⁷(He⁴, Be⁷)Na²⁴
RELATIVE NUMBER
1
2
3
4
5
0
2
4
6
8
10
12
14
16
18
Na²⁴ ENERGY (MEV)

distribution must be taken as an estimate only. From these results it is impossible to say whether or not there is a substantial contribution from the (He^4, α He^3) reaction. However, it is clear that there are large numbers of high energy Na^{24} recoils which could come only from the ejection of heavy particles, or the successive emission of light particles, into the backward hemisphere. This is not in disagreement with our expectations from the angular distribution of Be^7 fragments in Figure 12.

Figure 18 presents the angular distribution of Na^{24} recoils in the laboratory system. The target was 60 $\mu g/cm^2$ of Al on a gold backing. The solid line represents the average results of two determinations. The dotted line is from a single determination. An attempt was made to estimate the angular distribution of Na^{24} from the (He^4, α He^3) reaction. This was done by assuming that the reaction has a compound nucleus mechanism, that the anisotropy in the angular distribution between 0° and 90° in the C.M. system is 3:1, and that the α and He^3 particles are evaporated with a constant energy of about 5 Mev. The results of this estimate are given by the smooth curve in Figure 18. The area under the curve has been adjusted to correspond with the supposition that all of the excess Na^{24} comes from the (He^4, α He^3) reaction. The energy distribution estimate in Figure 17 assumed an

FIGURE 18

The angular distribution of Na^{24} recoils in the laboratory system. The solid experimental line is an average of two determinations. The dotted line is from one determination. The smooth curve is an estimate for the Al^{27} (He^4, α He^3) Na^{24} reaction and the dashed line is the result of subtracting the smooth curve from the experimental data.

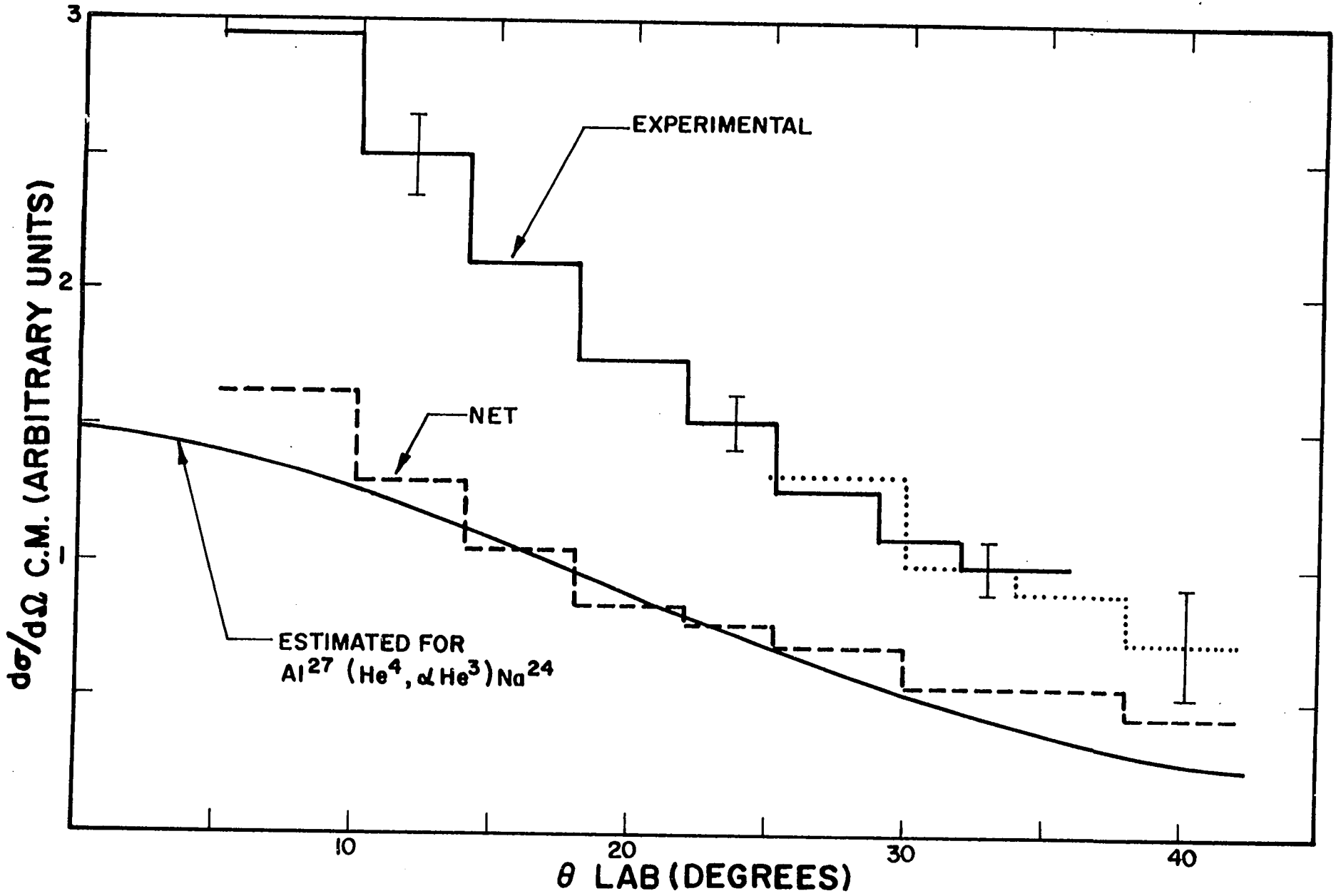
3
2
1
EXPERIMENTAL
NET
ESTIMATED FOR
Al27 (He4, α He3) Na24
dσ/dΩ C.M. (ARBITRARY UNITS)
10
20
30
40
θ LAB (DEGREES)

isotropic angular distribution in the C.M. system. However, the energy distribution in a narrow angular range is not sensitive to the shape of the angular distribution. The dashed line in Figure 18 is the result of subtracting the curve from the experimental data, and therefore represents the angular distribution of Na^{24} nuclei from the (He^4, Be^7) reaction corrected for an assumed yield from the (He^4, $\alpha\, He^3$) process.

The estimate for the angular distribution of the (He^4, $\alpha\, He^3$) reaction is based on reasonable assumptions but, at the same time, it is highly arbitrary. The most critical assumption is the 3:1 ratio for the anisotropy. A correction to the data based on an isotropic angular distribution for the (He^4, $\alpha\, He^3$) reaction would give a very steep angular distribution for the (He^4, Be^7) reaction. In principle, it would be possible to calculate the angular distribution of Na^{24} recoils from (He^4, $\alpha\, He^3$) reactions with good accuracy using a Monte Carlo program if the energy distributions and angular distributions of the individual α and He^3 particles were known. In the absence of this information the results of the foregoing analysis must be regarded as tentative.

In Figure 21 the corrected angular distribution of Na^{24} recoils, as given by the dashed line in Figure 18, has been transformed into the C.M. system and reflected about 90° for comparison with the Be^7 data. The transformation into the C.M. system was accomplished by using

the same kinematics as were applied to Be^7.

There are several experiments which should be attempted before the Na^{24} work may be considered a closed subject. In particular, it is desirable to extend the angular distribution information out to 60° and to measure the fraction of the total yield retained by the target. The angular distribution for the (He^4, Be^7) reaction should show a peak between 40° and 60° to which the (He^4, αHe^3) reaction should not contribute. Observation of this peak could form the basis for an estimate of the yield from the (He^4, αHe^3) reaction which would be independent of integral cross section measurements. Unfortunately, observations at large angles could be complicated by scattering in the target because of the low laboratory energy of the Na^{24} recoils and it may be necessary to ascertain the effect of target thickness on the angular distributions.

CHAPTER IV

DISCUSSION AND SUMMARY

A. Summary of the Data.

In general, the data agrees quite well with the predictions of the compound nucleus theory of nuclear reactions. This conclusion is supported chiefly by three pieces of evidence. First, as seen from an examination of Tables 1 and 2, a large fraction of the Be^7 yield is found in the backward hemisphere. The ratio of Be^7 activity found in the forward hemisphere to that found in the backward hemisphere, in the C.M. system, is 1.1 ± 0.1 for oxygen. This is an average value for two runs. It would be very unlikely for the yield from direct interactions to divide equally about 90° The forward-backward ratio for aluminum targets is not as well known because of the large error limits on the data. The first determination (run number one) is believed to be the most accurate because the target was thicker than the targets used in succeeding runs, and this tended to suppress the background problem. Also, there is good agreement between the total observed activity and the expected activity, calculated from the integral cross section and beam exposure. Run number one gives a value of 1.6 ± 0.5 for the forward-backward ratio for aluminum. The errors in these ratios are taken from Tables 1 and 2.

Second, the angular distributions of Be^7 fragments from oxygen and aluminum are strongly suggestive of a compound nucleus mechanism. The angular distribution from oxygen could not be measured in the backward hemisphere and the data for aluminum is very uncertain in the forward hemisphere, but, taken together, the two studies complement each other nicely if we make the assumption that the same mechanism is responsible for both reactions. The magnitudes of the asymmetries, as we shall see in Section C, are not out of line with theoretical estimates based on a statistical model.

The energy distribution data for both oxygen and aluminum targets supplies the third piece of evidence. The fits to evaporation theory in Figures 5 and 11 should be taken with a measure of reserve, but even so, the general shapes of the energy distribution histograms are what we expect from compound nucleus theory. The number of fragments increases with decreasing energy until the coulomb barrier is reached and begins to inhibit the reaction. It is worth noting that the energy distributions were obtained at small forward angles where any contribution from direct interactions should be the most obvious.

Unfortunately, there are very few parallel investigations with which this work may be compared. Bouchard (6-160) and Lindsay (22-2168) have pioneered the study of Be^7 production in the medium energy region, but their experiments are largely introductory in nature. Lindsay

has measured the forward-backward ratio and ranges of Be^7 fragments from a magnesium target and his results are in qualitative agreement with the compound nucleus hypothesis. On the basis of a similar forward-backward measurement, Bouchard concluded that the reaction could not go through a compound nucleus. Lindsay has also shown that theoretical cross sections for Be^7 production from aluminum, using the statistical model as a basis for calculation, are in reasonable agreement with measured values.

The processes responsible for heavy fragment production at high energies, several hundred Mev to 2 Bev, are still largely a matter of conjecture Hudis and Miller (19-1322) and Dostrovsky, et al (9-1659) have used the statistical model to calculate cross sections for fragments heavier than He^4 with fair results. Katcoff (21-905) has analyzed the energy distributions and angular distributions of Li^8 fragments from 2.2 Bev proton bombardments in terms of a compound nucleus mechanism. To summarize the evidence from high energy experiments, it seems fair to say that some, but not all, of heavy fragment production can be accounted for by the compound nucleus theory. However, some other process also seems to play a role. The generality of the statistical theory would indicate that if heavy fragment production at high energies goes through a compound nucleus, then the same must be true in the medium energy region, and to this extent the high

energy work is in agreement with the conclusions of this study.

B. Cross Section Comparisons.

If the compound nucleus is important in the production of Be^7, then it should be possible to account for the observed variations in cross section with target element. We have already noted that Lindsay (22-2168) found the cross sections for aluminum targets to be in reasonable agreement with theoretical values. The aim here will be to extend this analysis to the other elements for which cross section data is available. Our approach will be one of estimation, rather than exact calculation, because the statistical theory itself, when applied to elements as light as those encountered in this work, is only an approximation. Furthermore, only relative cross sections will be considered, that is, we wish to account only for the variation of cross section with target element. Using the statistical assumption, the cross section for Be^7 production may be written[1]:

$$\sigma_{Be^7} \sim \sigma_c \frac{gm \int E\, \sigma_I(E^*)\, \rho(E^*)\, dE}{\sum_i g_i m_i \int E_i\, \sigma_I(E_i^*)\, \rho(E_i^*)\, dE_i}$$

Where the quantities in the numerator refer to Be^7 and the summation

[1] See reference (11-425) for an excellent review of the statistical theory.

is carried out over all particles, i, which may be emitted from the compound nucleus. The level density of the residual nucleus, $\rho(E^*)$, at an excitation energy E^*, will here be taken as exp. $2(aE^*)^{1/2}$. If the indicated integration is carried out, the result is f(E) exp. $2(aE)^{1/2}$ where E is now the maximum excitation energy of the residual nucleus. It is assumed that only the exponential in E is important in determining relative cross sections. It is further assumed that Be^7 emission is in competition with only one other particle, b, which is not necessarily a neutron, but is selected as the most competitive particle from each compound nucleus. The cross section may now be written:

$$\sigma_{Be^7} \sim \text{const.} \frac{\text{exp. } 2(a\,E_{Be^7})^{1/2}}{\text{exp. } 2(aE_b)^{1/2}}$$

$$\sim \text{(const.) exp. } 2a^{1/2}\,(E_{Be^7}{}^{1/2} - E_b{}^{1/2})$$

$$\sigma_{Be^7} \sim \text{(const.) exp. } (S_{Be^7} - S_b)$$

For convenience, $S = 2\,(aE)^{1/2}$ and a is assumed constant for each target element. E is simply equal to $(E_\alpha + Q - V)$ and may be regarded as the energy available to the fragment or competing particle. E_α is the energy of the incident helium ion in the C.M. system and

$$V = Z_1\,Z_2\,e^2/\,(R_1 + R_2).$$

The evaporated particle for which E_b was largest was used in the

calculations. The parameter a is taken as A/10 with A equal to the mass number of the target nucleus.

Now a plot of log σ_{Be^7} against $(S_{Be^7} - S_b)$ should be a straight line, which is the simple relation we are looking for. The extent to which this is true is shown in Figure 19. Data for Mg, Al, Ti, Co and Cu are from Lindsay (22-2168). Cross sections for target elements which contained more than one isotope were corrected for isotopic abundances as follows. The quantity $(S_{Be^7} - S_b)$ was determined for all isotopes of a given target element which were present in amounts greater than 1%. Then $(S_{Be^7} - S_b)$ was plotted as a function of log σ_{Be^7} for all monoisotopic targets. Nitrogen and oxygen were considered monoisotopic for this purpose. The slope of the straight line drawn through these points was used to estimate the contribution to the total cross section from each isotope of a polyisotopic target, relative to the contribution from the most abundant isotope. These relative contribution factors were used as weighting factors for the isotopic abundances. Finally, the observed cross section of a polyisotopic target was divided by the sum of the adjusted percent abundances of the isotopes present. As an example, take the case of Cu. There are two isotopes, Cu^{63} and Cu^{65}, with abundances of 69% and 31% respectively. The above analysis indicated that the contribu-

FIGURE 19

Cross sections plotted against $(S_{Be^7} - S_b)$. The data for Mg, Al, Ti, Co and Cu are from Lindsay.

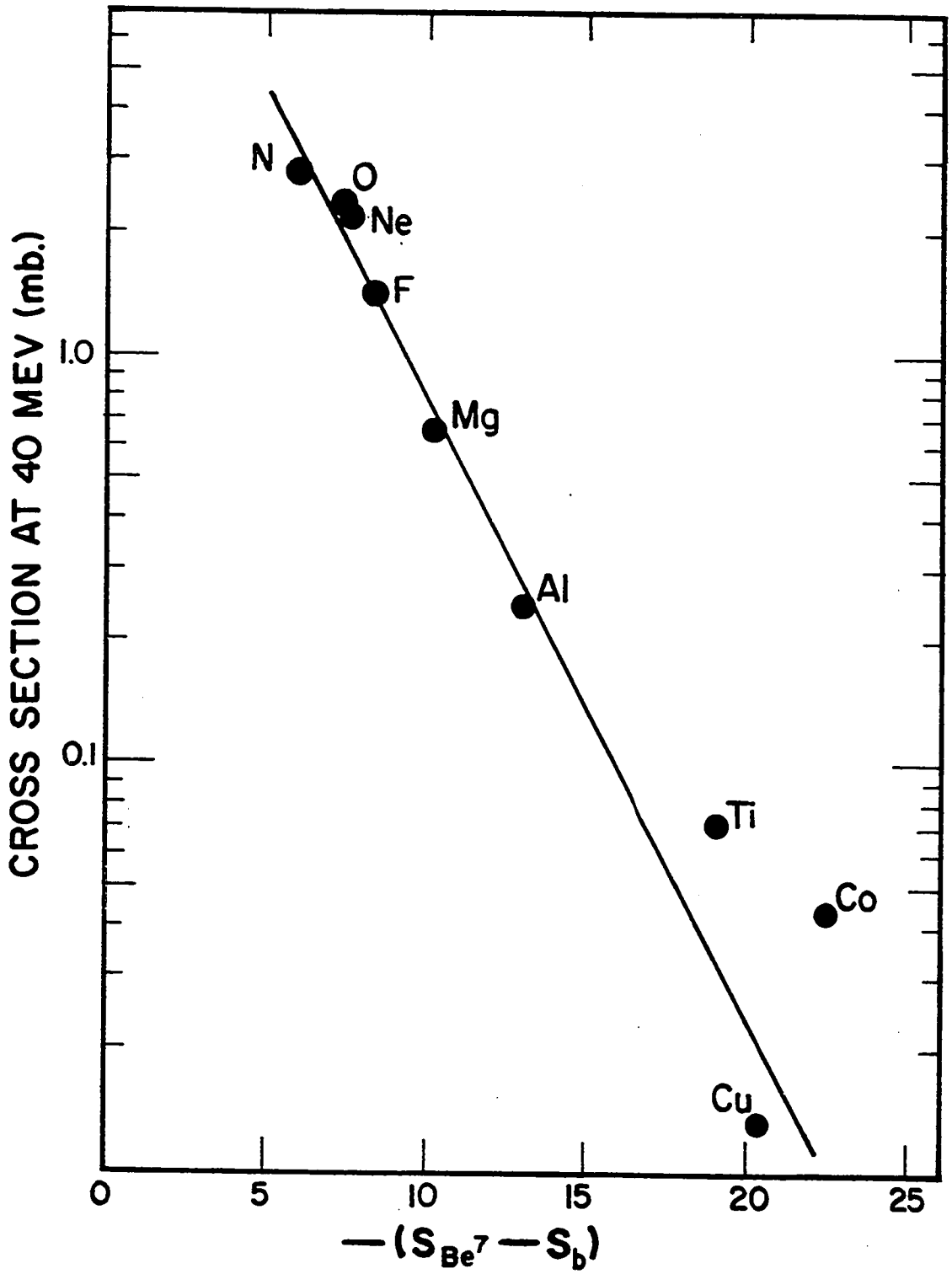
CROSS SECTION AT 40 MEV (mb.)
1.0
0.1
N
O
Ne
F
Mg
Al
Ti
Co
Cu
0
5
10
15
20
25
—(S_Be7 — S_b)

tion from Cu^{65} relative to Cu^{63} was negligible. The weighting factor for this isotope was therefore zero, and the observed cross section was divided by 0.69 because only 69% of the target contributed to the total cross section. The cross sections of Ne, Mg, Ti and Cu were adjusted in this manner. These adjusted cross sections were then plotted as a function of $(S_{Be^7} - S_b)$ for the most abundant isotope, along with the points for monoisotopic targets, and the best locus of the straight line was re-determined.

The fit is very satisfactory except for Ti and Co. The presence of small amounts of oxygen and nitrogen in these targets could easily account for the discrepancy. Titanium is especially difficult to obtain without traces of oxygen and nitrogen. Also, the precision on the measurements for cobalt is poor.

It is worth noting that a plot of log σ_{Be^7} against S_{Be^7} produces a rather poor fit to a straight line. The use of the competition term, S_b, gives better results. Carbon is not included in this analysis because of the probability that Be^7 is left as a spallation residue of carbon targets.

C. Angular Distributions.

I. Halpern (16-510) has proposed a classical model to describe the angular distributions of evaporated particles in compound nucleus reactions. The model assumes that the evaporation of particles, or

fragments, takes place from a rotating sphere filled with a Maxwell gas and that the rate of emission per unit surface area is proportional to the pressure on that element of area. The resulting expression for the angular distributions with respect to the beam direction is

$$\frac{d\sigma}{d\Omega} \propto \exp\ (-X \sin^2 \theta)\, J_o\, (iX \sin^2 \theta)$$

This is identical with the expression offered by Ericson and Strutinski (10-284) in its classical limit. J_o is a zero order Bessel function and

$$X = \frac{\frac{1}{2}\, m\, R^2_{Be^7}\, \bar{\omega}^2}{2T}$$

R_{Be^7} is the effective radius between the fragment and the residual nucleus during the evaporation process, m is the reduced mass of the fragment, $\bar{\omega}$ is the average angular velocity of the compound nucleus, and T is the nuclear temperature. In Figures 20 and 21 this function is compared with the experimental angular distributions of Be^7 fragments from oxygen and aluminum for various values of the parameter X. The experimental plot for oxygen in Figure 20 was obtained by visually averaging the histogram in Figure 7. The histogram labelled "Na^{24}" in Figure 21 is the angular distribution of the Na^{24} residual nucleus in the forward direction reflected about 90°. The assumption implicit in doing this is that the forward moving Na^{24} is the complement of

FIGURE 20

A comparison of theoretical angular distributions based on a statistical model with the angular distribution of Be^{7} fragments from oxygen. The experimental curve was obtained by visually averaging the histograms in Figure 7.

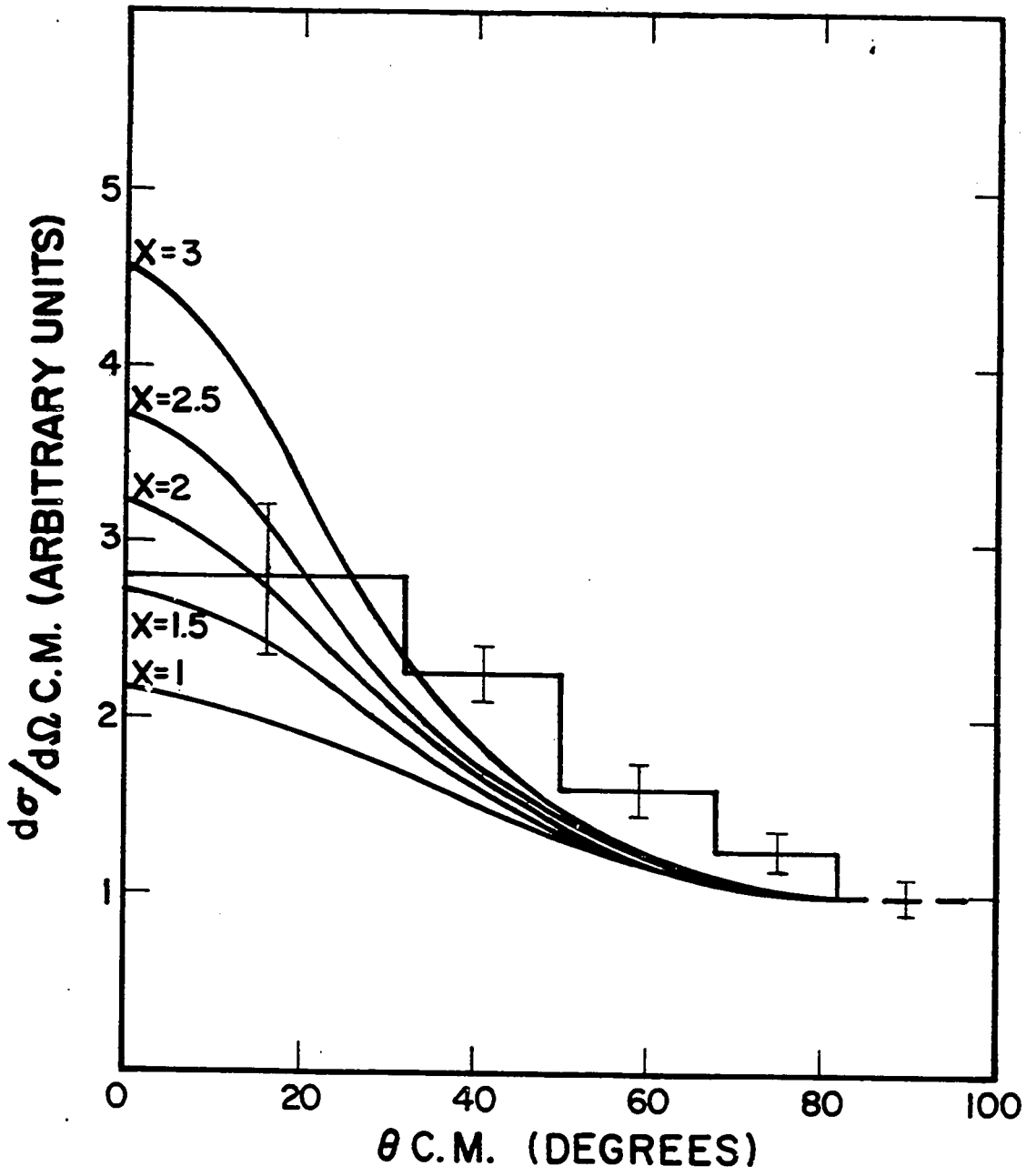
dσ/dΩ C.M. (ARBITRARY UNITS)
θ C.M. (DEGREES)
X=3
X=2.5
X=2
X=1.5
X=1
0
20
40
60
80
100
1
2
3
4
5

FIGURE 21

A comparison of theoretical angular distributions based on a statistical model with the angular distribution of Be^7 fragments from aluminum. The Be^7 data are the same as those of Figure 12. The Na^{24} angular distribution was described in Chapter III, Section H.

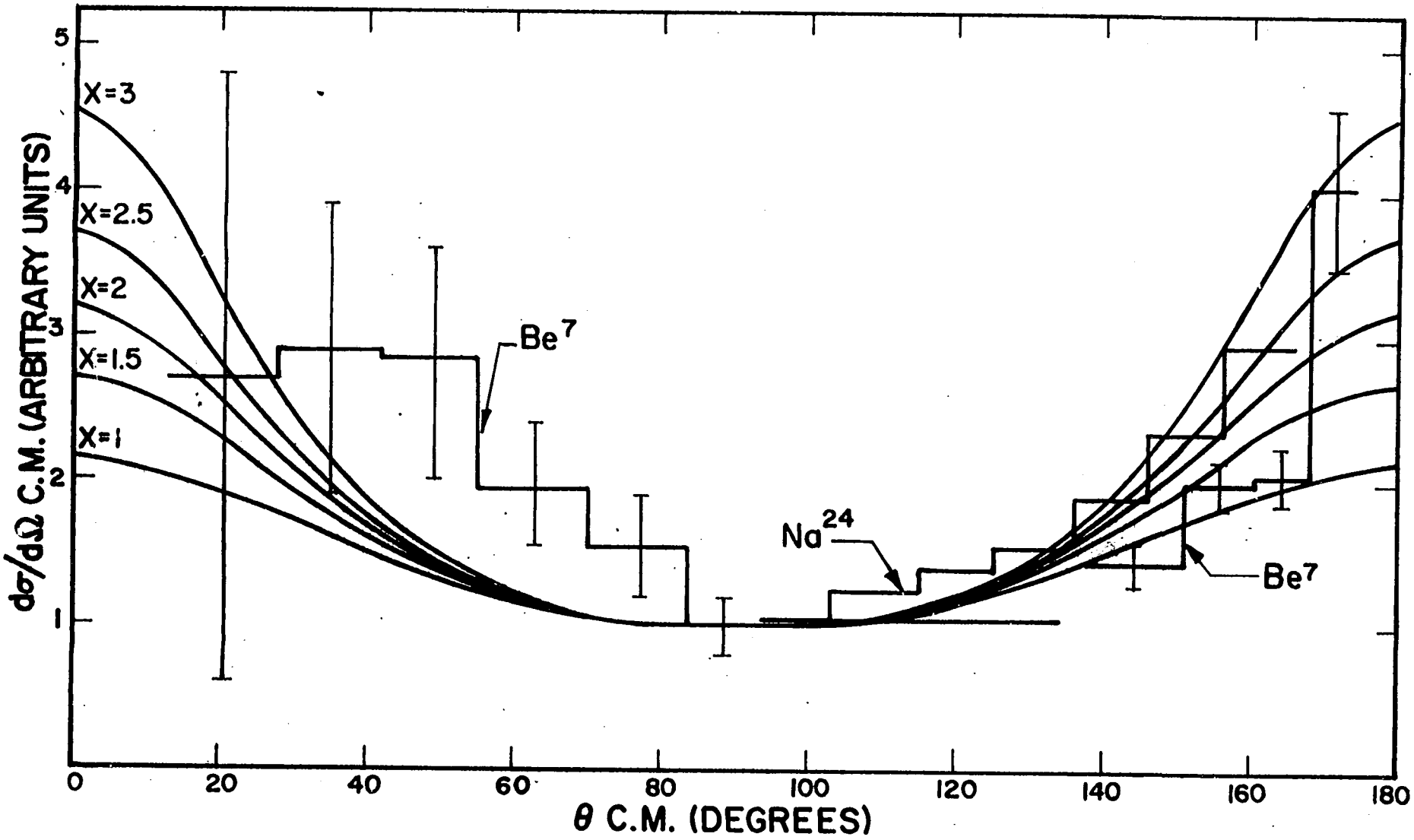
X=3
X=2.5
X=2
X=1.5
X=1
Be7
Na24
Be7
dσ/dΩ C.M. (ARBITRARY UNITS)
θ C.M. (DEGREES)
0
20
40
60
80
100
120
140
160
180
1
2
3
4
5

the backward moving Be^7 fragments. The Na^{24} data are corrected for a likely contribution to the Na^{24} yield from the (He^4, α He^3) reaction and must be regarded as tentative (see Section H of Chapter III).

The agreement with the aluminum data in the backward hemisphere is satisfactory but in the forward hemisphere for both oxygen and aluminum there seems to be too much yield in the vicinity of 90°. It is not known whether this represents a mis-application of the model or an inadequacy of the experimental technique. In any case, the magnitudes of the observed anisotropies are not out of line with the predictions of the model, provided that a value for X of 2 or 2.5 is reasonable for these reactions.

An estimate for X may be obtained as follows. We consider the oxygen reaction first. The target nucleus is struck by a 42.5 Mev helium ion and forms a compound nucleus, Ne^{20}. The compound nucleus then ejects a Be^7 fragment and leaves behind C^{13}. The average angular velocity of the compound nucleus, $\bar{\omega}$, is simply the average angular momentum divided by the moment of inertia:

$$\bar{\omega}^2 = \frac{\bar{J}^2}{I^2} = \frac{m_\alpha R_\alpha^2 (E_\alpha - V_\alpha)}{(2/5\, M_p A R^2_{C.N.})^2}$$

The subscript α refers to the incident helium ion. R_α is the interaction radius effective in the formation of the compound nucleus.

The rigid body moment of inertia has been used. $R_{C.N.}$ is the radius of the compound nucleus and $m_p A$ is its mass. Substituting this expression into the equation for X yields

$$X_O = 1.2 \frac{R_\alpha^2 R_{Be^7}^2}{R_{C.N.}^4}$$

for oxygen targets. The nuclear temperature was obtained from $T = (E/a)^{1/2} = 2$ Mev, with $a = A/10$. The coulomb barrier for the helium ion was calculated from $V = Z_1 Z_2 e^2 / (R_1 + R_2)$. The choices of the correct values for the various R's is a difficult problem. R_{Be^7} and $R_{C.N.}$ are probably rather large, while R_α should be on the small side because of the transparency of the nuclear surface to the incident helium ion. Evidence suggests (20-1965) that $R_\alpha \sim r_\alpha 16^{1/3} + 1.8 \times 10^{-13}$ with $r_\alpha = 1.2 \times 10^{-13}$ cm is a good approximation. For R_{Be^7} and $R_{C.N.}$ we first try $r_{Be^7}(13^{1/3} + 7^{1/3})$ and $r_{C.N.} 20^{1/3}$ respectively. With $r_{Be} = r_{C.N.} = 1.3 \times 10^{-13}$ cm, X_O becomes 2.6. A similar computation for aluminum, using $r_{C.N.} = 1.3 \times 10^{-13}$ cm, gives a value of about 2.3 for X_{Al}. It is not suggested that these are necessarily the best values for R_α, R_{Be^7}, and $R_{C.N.}$ The intent here is only to show that reasonable choices for the various R's give reasonable values of X with respect to the observed anisotropies.

There are several effects which this simple analysis does not take into consideration. In the first place, the model does not take

into account coulomb effects. The coulomb forces between the Be^7 fragments and the residual nucleus will tend to force the fragments along trajectories which are perpendicular to the surface of the residual nucleus. If the Be^7 fragments are preferentially emitted from the equator of a rotating nucleus, the coulomb forces would enhance the anisotropies and therefore tend to increase X. Also, the rigid body value for the moment of inertia may be too large. A share of the energy of rotation is probably distributed in the motions of single nucleons and collective motions of a few nucleons. These effects tend to reduce the moment of inertia from its rigid body value, and hence tend to increase X. C. Gruhn (15-97) has found the moment of inertia to be less than the rigid body value for the compound nucleus Zn^{62}, formed in the helium ion bombardment of Ni^{58}. The extent of the deviation is not well known at this time.

The use of the rigid body moment of inertia in estimating X gives values which tend to be on the large side when compared with the observed angular distributions. The inclusion of coulomb effects would make X still larger. Therefore, the results of this work do not indicate a large deviation of the moment of inertia from its rigid body value, assuming that the application of Halpern's model to these data is valid.

The large anisotropies which should be found in the angular distributions of heavy fragment reactions, assuming they go through a compound nucleus, make them a sensitive tool for studying the properties of a rotating nucleus. Unfortunately, this advantage is offset by the low cross sections that may be expected for these reactions.

D. Concluding Remarks.

The results of this study indicate that the compound nucleus plays a dominant role in the production of Be^7 from the helium ion bombardment of oxygen and aluminum. Statistical theory is capable of accounting for these results, at least in a semi-quantitative way. These conclusions, to the extent that they are correct, further demonstrate the generality and usefulness of the theory. On the basis of these results, one may surmise that the compound nucleus is important in many heavy fragment reactions.

This does not mean that direct interactions are unimportant. The catcher foil technique is particularly sensitive to compound nucleus reactions and a substantial direct interaction contribution to the cross sections could have gone undetected. Indeed, the experiments of Nicholson and Hower (Appendix II) on Be^7 from carbon, and the results of Zafiratos (33) on Li^6 fragments from nitrogen, indicate that direct interactions are taking place.

The experiments described in this work are difficult, and in some instances marginal. Corroborative evidence should be obtained, especially by means of altogether different experimental approaches from those used here. In particular, one would like to look at heavy fragment production from the medium weight elements where statistical theory could be applied with more confidence. This predicates the use of higher beam energies than are currently available at this laboratory in order to overcome the large coulomb barriers to heavy fragment emission. One class of experiments where heavy fragment production should be particularly favorable is heavy ion bombardments. These reactions form highly excited compound nuclei with large amounts of rotational energy. Heavy fragments should compete more favorably with the emission of light particles because of the desire on the part of the nucleus to get rid of as much angular momentum as possible.

APPENDIX I

Ranges of Be^9 Ions in Au and Al

Experimental

Range-difference curves have been measured for Be^9 ions in gold and aluminum in the energy range 2 to 21 Mev. The Be^9 ions were produced in the 60-inch scattering chamber of the University of Washington cyclotron by elastically scattering helium ions from a beryllium target. Pulse height measurements of the Be^9 recoils, degraded by various thicknesses of gold or aluminum foil, served as the basis for determining range-difference curves. Extrapolation of these curves to zero energy permits transformation of the data into the more useful range-energy relationship.

Two counters were used. The Be^9 recoil detector was a 5000 ohm silicon, diffused type, solid state counter with a bias of 20 volts. It was used in conjunction with a low noise Tennelec pre-amplifier. The elastically scattered helium ions were detected with a CsI (Tl) crystal and photomultiplier assembly. Coincident pulses from both counters were displayed on two 20 channel pulse height analyzers. The solid state counter was calibrated on Be^9 recoils, the energy being calculated from kinematic considerations. The

energy of the recoils was changed by varying the angle of observation. The absolute energy scale of the calibration was checked by looking at the 6.05 and 8.78 Mev α particles from a Pb^{212} source. The α particle points were 400 Kev above the Be^{9} calibration curve. Since the average energy loss of Be^{9} recoils in the 0.3 mg /cm^2 target was estimated to be about 400 Kev, the agreement was considered satisfactory.

Gold and aluminum foils were interposed between the beryllium target and the solid state counter by means of a remotely operated degrader wheel. The unit thickness of the foils was 2.28 ± 0.07 mg/cm^2 for gold and 1.60 ± 0.04 mg/cm^2 for aluminum. The degraders consisted of stacks of these unit foils from 1 to 8 foils thick. The thickness of each foil was determined be weighing, but no investigation was made of thickness uniformity within a foil. However, the practice of using the foils in stacks tended to average out any thickness non-uniformities.

The energy of the degraded Be^{9} recoil was determined by taking the center of the pulse height distribution, in channels, and converting to energy units by means of the calibration curve. Range-difference curves were obtained simply by plotting the energy of the degraded recoil against the thickness of the degrader. As the thickness of the degraders was increased, the width of the pulse height distributions increased rapidly. This was believed to be due to a scattering effect,

the result of the geometry between target, degraders and detector. For this reason it was not feasible to degrade a 21 Mev recoil all the way down to 2 Mev, the useful threshold of the detection system. Instead, the energy of the undegraded recoil was decreased in several steps by changing the angle of observation. The result was a series of overlapping range-difference curves, typified by the following sequence of energy limits: 21 - 5.6 Mev, 17.9 - 3.4 Mev, 14.8 - 2.3 Mev, 8.9 - 2.2 Mev, 5.2 - 2.7 Mev. This series of curves was then fitted together to form a single range difference curve in the energy interval 21 - 2.2 Mev.

Results

The range-difference curves for Be^9 ions in gold and aluminum are given in Figures 22 and 23 respectively. The error limits on the data points are composites of uncertainties in determining the calibration curve, the centers of pulse height distributions, and the thickness of degraders. There are three points on the range-difference curve for gold which are too low. Each of these points represents Be^9 recoils degraded by 7 or more thicknesses of gold foil. The pulse height distributions for these recoils was very broad and it is felt that there was some systematic error involved in their interpretation. The error limit on the energy axis indicates the uncertainty in the absolute

values of the energy. It is composed of an uncertainty of ± 200 Kev in the beam energy and ± 0.3° in the angle of the Be^9 counter. The error limit on the range axis is the estimated uncertainty in extrapolation of the curve to zero energy.

The corresponding range-energy curves are shown in Figures 24 and 25 for gold and aluminum respectively. The error limits shown represent uncertainties in the absolute values of the energy and extrapolation of the range-difference curves. These errors are believed to be larger than those involved in the measurements. The circled points in the figure for aluminum are the estimates of L. C. Northcliffe (27), included here for comparison. Northcliffe's work is most accurate for much greater ion energies, and with this in mind, the agreement is considered to be satisfactory. The single circled point on the range-energy curve for gold is from a radiochemical measurement by A. W. Fairhall (12) of the range distribution of monoenergetic Be^7 ions from the $He^3(He^4, \gamma)Be^7$ reaction. Northcliffe's work (28-1744) on B^{10} and B^{11} ranges indicates that Be^7 may be expected to have a range about 3% greater than that of Be^9 in this energy region. Thus, the range-energy curve for Be^9 should be displaced upward by 3% for purposes of comparison with the solitary point for Be^7. The agreement is still very reasonable.

FIGURE 22

The range-difference curve for Be^9 ions in gold. The error limits on the data points are composites of uncertainties in the calibration curve, the centers of pulse height distributions, and the thickness of degraders. The error limit on the energy axis indicates the uncertainty in the absolute values of the energy. The error limit on the range axis is the estimated uncertainty in extrapolation of the curve to zero energy.

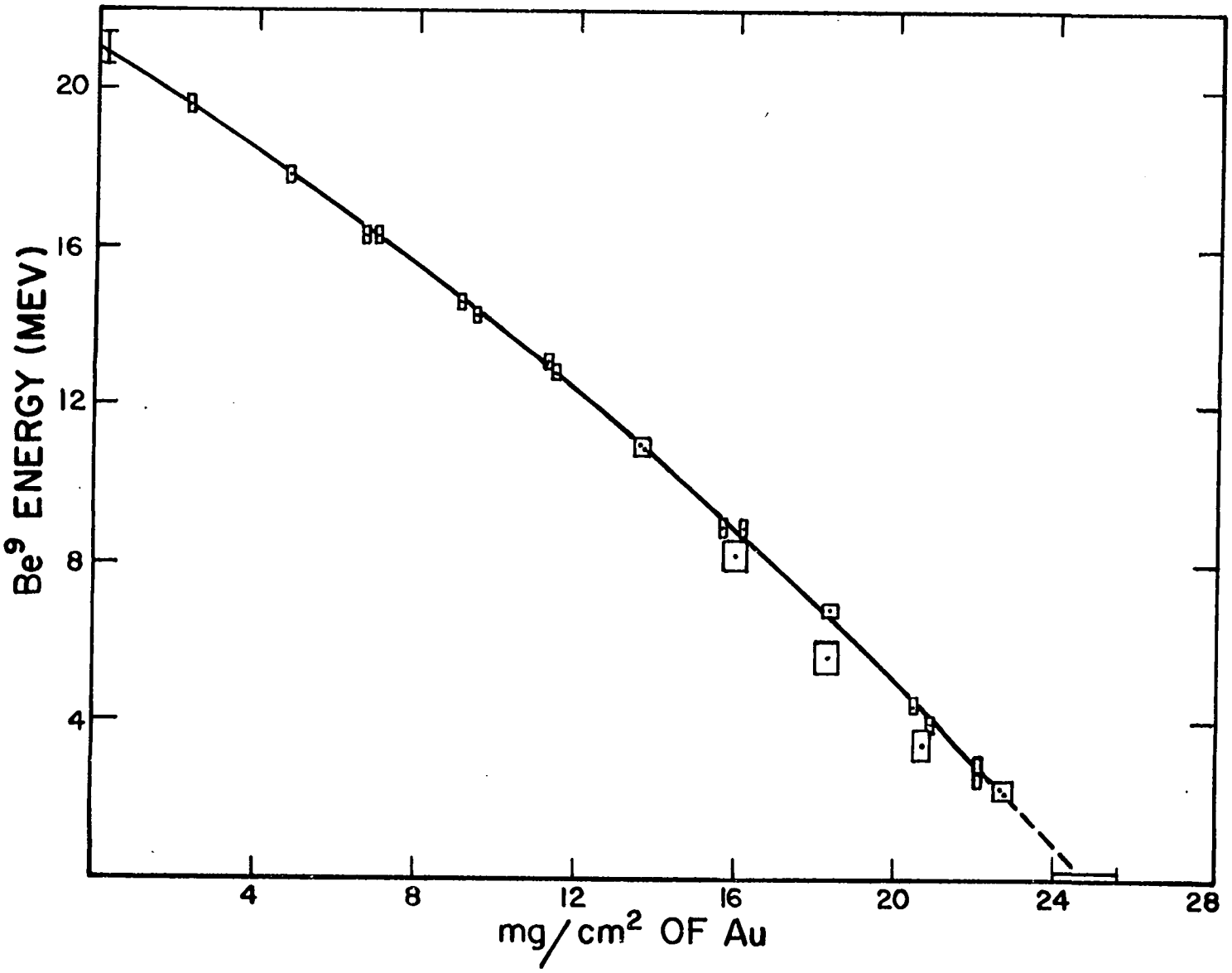
Be⁹ ENERGY (MEV)
20
16
12
8
4
4
8
12
16
20
24
28
mg/cm² OF Au

FIGURE 23

The range-difference curve for Be^9 ions in aluminum. The error limits on the data points are composites of uncertainties in the calibration curve, the centers of pulse height distributions, and the thickness of degraders. The error limit on the energy axis indicates the uncertainty in the absolute values of the energy. The error limit on the range axis is the estimated uncertainty in extrapolation of the curve to zero energy.

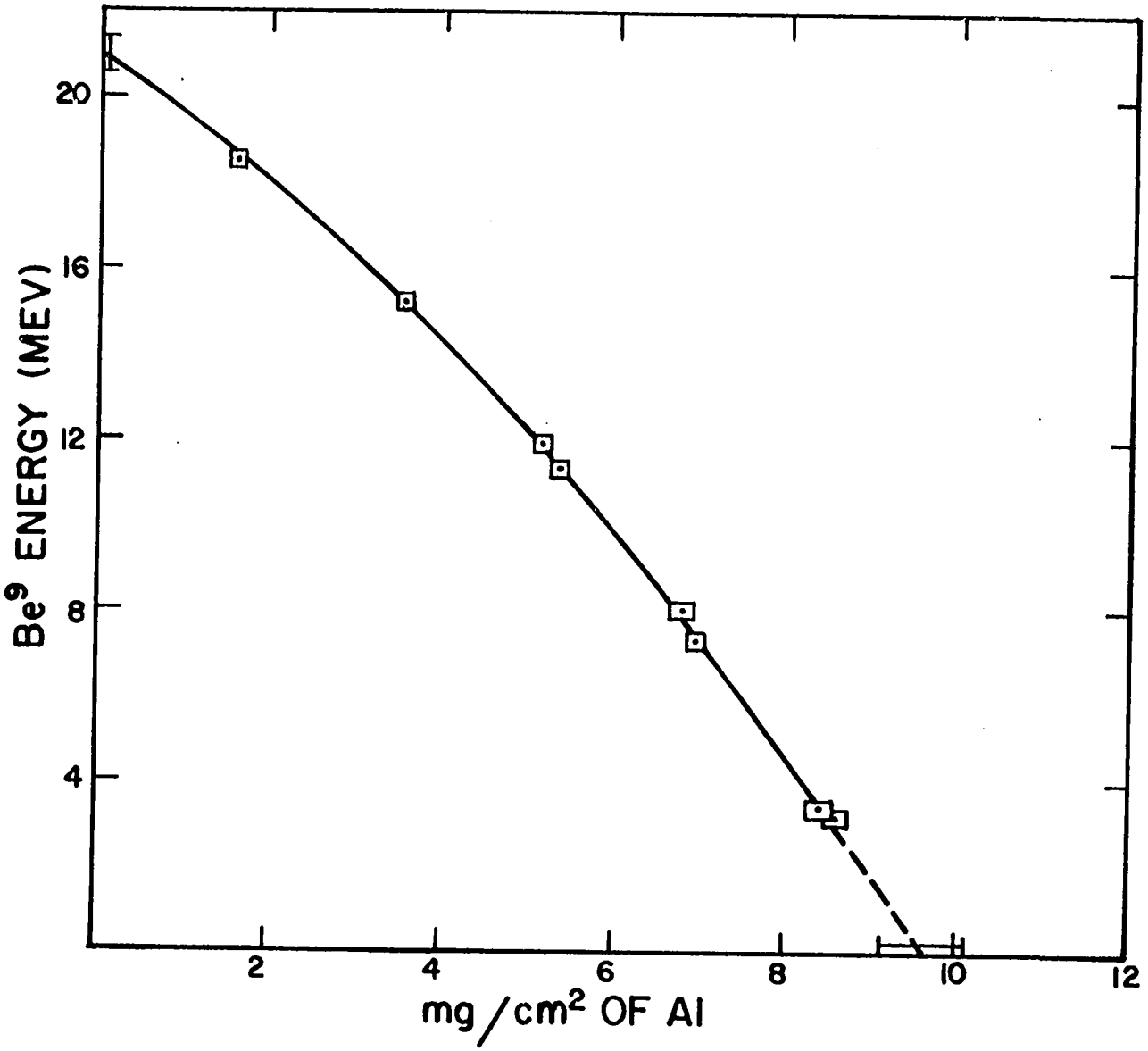
20
16
12
8
4
Be⁹ ENERGY (MEV)
2
4
6
8
10
12
mg/cm² OF Al

FIGURE 24

The range-energy relation for Be^9 ions in gold. The error limits represent uncertainties in the absolute values of the energy and extrapolation of the range-difference curve. The circled point is from a radiochemical measurement by A.W. Fairhall of the range distribution or monoenergetic Be^7 ions from the He^3 (He^4, γ) Be^7 reaction.

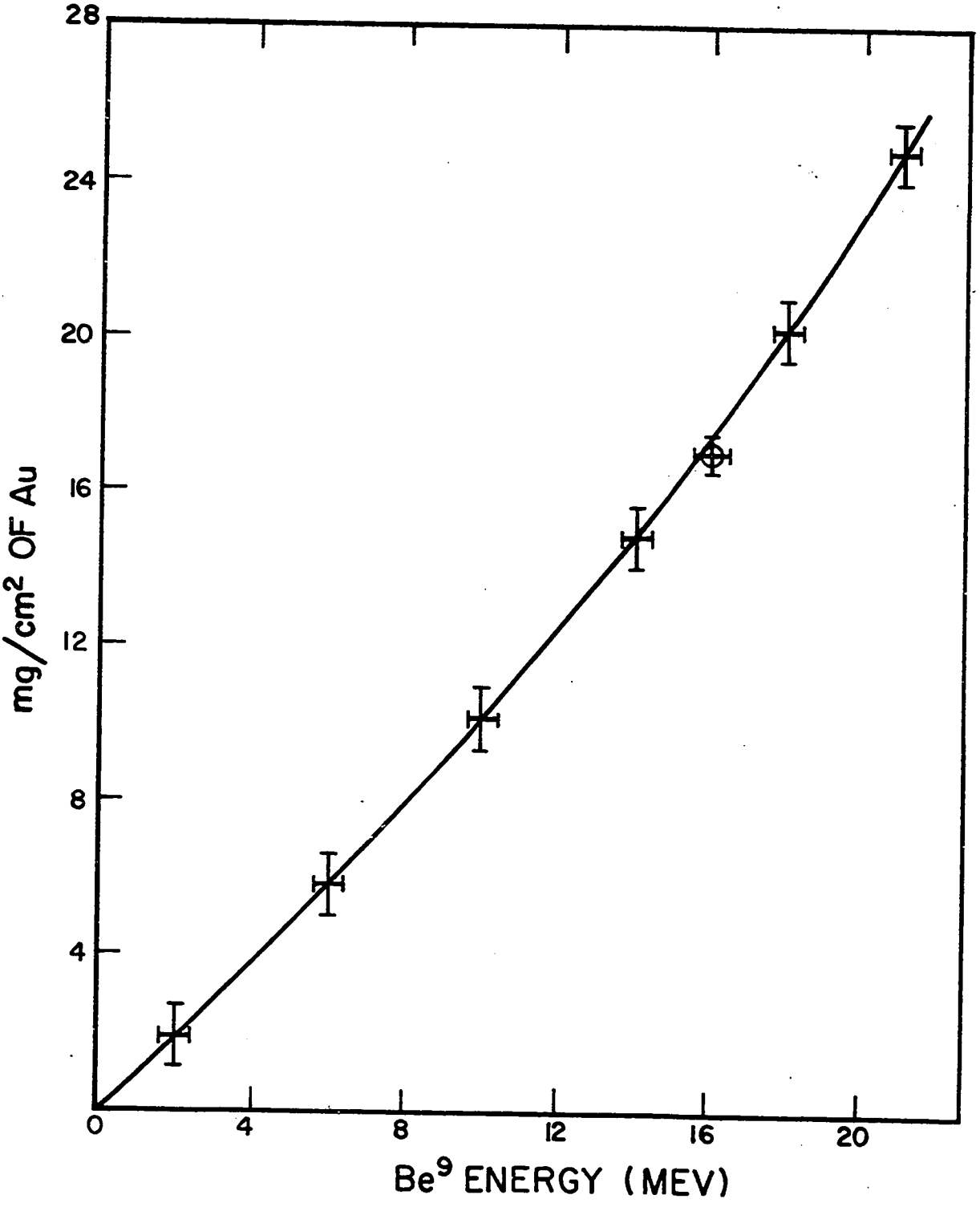
28
24
20
16
12
8
4
0
4
8
12
16
20
mg/cm² OF Au
Be⁹ ENERGY (MEV)

FIGURE 25

The range-energy relation for Be^9 ions in aluminum. The error limits represent uncertainties in the absolute values of the energy and extrapolation of the range-difference curve. The circled points are taken from an estimate of Be^9 ranges in aluminum by L. C. Northcliffe.

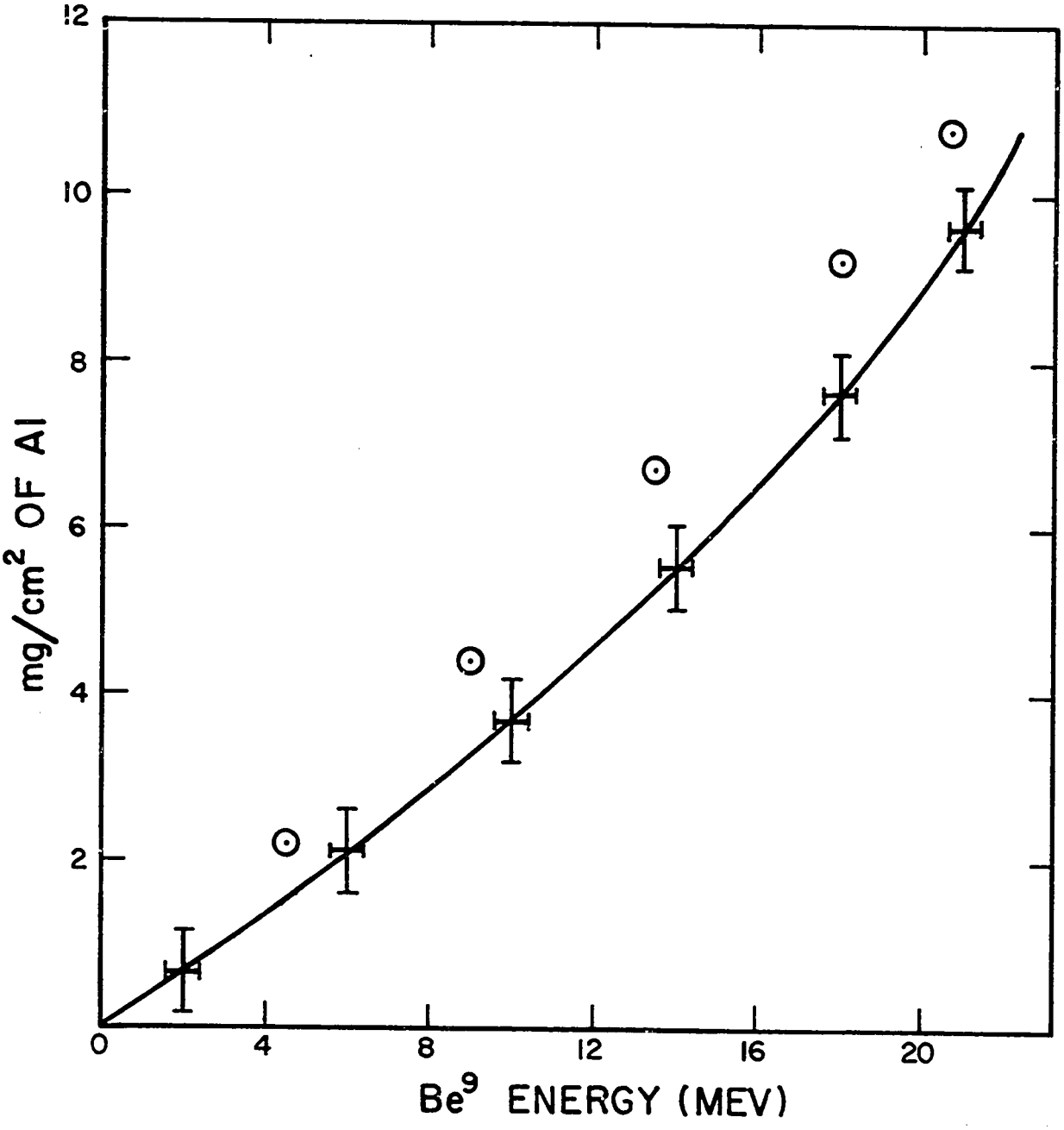
12
10
8
6
4
2
0
4
8
12
16
20
mg/cm² OF Al
Be⁹ ENERGY (MEV)

APPENDIX II

Counter Experiments

In 1959 and 1960 a series of counter experiments was made in collaboration with Dr. William Nicholson. The object of these experiments was to study heavy fragment production in the helium ion bombardment of light elements. A counter has the obvious advantage over chemical techniques of being able to look at non-radioactive fragments which might be expected in greater abundance because of the generally more favorable Q values. Also more detailed measurements may be made with a counter. These experiments were deferred when continuing radiochemical measurements made it apparent that the bulk of the yields, at least for Be^7 production, were at low fragment energies and large angles, regions which the counter could not explore because of its high threshold energy for detection of fragments. A description of the counter and some of the results obtained with it are given here as a possible guide to future work. These experiments were of a preliminary nature and the results must be regarded in that light.

The counter was a gridded ionization chamber with three collector plates as shown schematically in Figure 26 . Particles entered the narrow end of the chamber through a thin nickel window. The

tapered shape permitted the chamber to be used at small angles with respect to the beam. The first two plates were used to identify the particles and measure their energies. The third plate was intended to be used in an anticoincidence circuit to discriminate against α particles; it was found to be unnecessary. The ionization chamber was filled with 30 to 60 cm of 90% argon - 10% methane. The choice of pressure depended on the heavy fragment to be detected and the energy range which was to be observed. Operating voltage was usually about 500 volts. The counter was used in a 60" scattering chamber. Accessory equipment consisted of preamplifiers, linear amplifiers and two 20 channel analyzers. One of the difficulties encountered was finding preamplifiers with sufficiently low noise characteristics to operate on the low voltage output pulses of the counter.

Calibration was accomplished by looking at elastically scattered recoils from 42-Mev helium ions incident on Li, Be, B and carbon targets. For calibrations the ionization chamber was gated by a separate α particle detector which counted the elastically scattered helium ions. By varying the angle between the two counters any desired recoil energy between about 5 Mev and 25 Mev could be obtained. It was found that the ionization chamber could easily separate

ions of different elements but could not adequately distinguish between isotopes of the same element. Some typical particle identification curves are shown in Figure 27 . The curves for Li^7 and Be^9 fold back when the ions have sufficient energy to traverse the entire length of the first two plates. In actual observations on heavy fragment production particle identification was not as clean as Figure 27 indicates. This is probably because several isotopes of any given element were observed. Improved resolution with respect to particle identification would have been advantageous.

Data on heavy fragments were obtained by gating the pulses from the front plate with pulses in a selected pulse height interval from the second plate. Pulse height spectra of heavy fragments were obtained by moving the gating interval over the energy range of interest. Some typical spectra from a carbon (polystyrene) target are shown in Figures 28 and 29 . The lower curve in Figure 29 shows the spectrum of pulses from the front plate that are in coincidence with pulses from the second plate which come in channel 14. The peaks can be associated with Be, B and C on the basis of the calibration. If a lower energy gate had been used a peak for Li ions would also have been observed.

The most extensive measurements were made with carbon targets.

Figure 30 presents spectra of Be ions from carbon at several angles. The high energy peak may be associated with the ground state transition in the reaction C^{12} (He^4, Be^7) Be^9. The movement of the peak toward lower energies as the angle increases is quantitatively consistent with the kinematics of the reaction. The transition to the second excited state of Be^9 is not evident in these data although it was observed in an earlier run. This may be because the counter exhibited better resolution in the earlier run. There are no further data worth reporting. However, it is important to note that Li and B fragments were also observed from carbon. Li and Be were obtained from the helium ion bombardment of aluminum and Be was observed from oxygen. Lithium fragments from both carbon and aluminum were about ten times as abundant as Be fragments. The yields from aluminum were much less than the yields from carbon or oxygen.

FIGURE 26

Diagram of the collector plate configurations of the ionization chamber.

ION CHAMBER COLLECTION PLATE CONFIGURATION

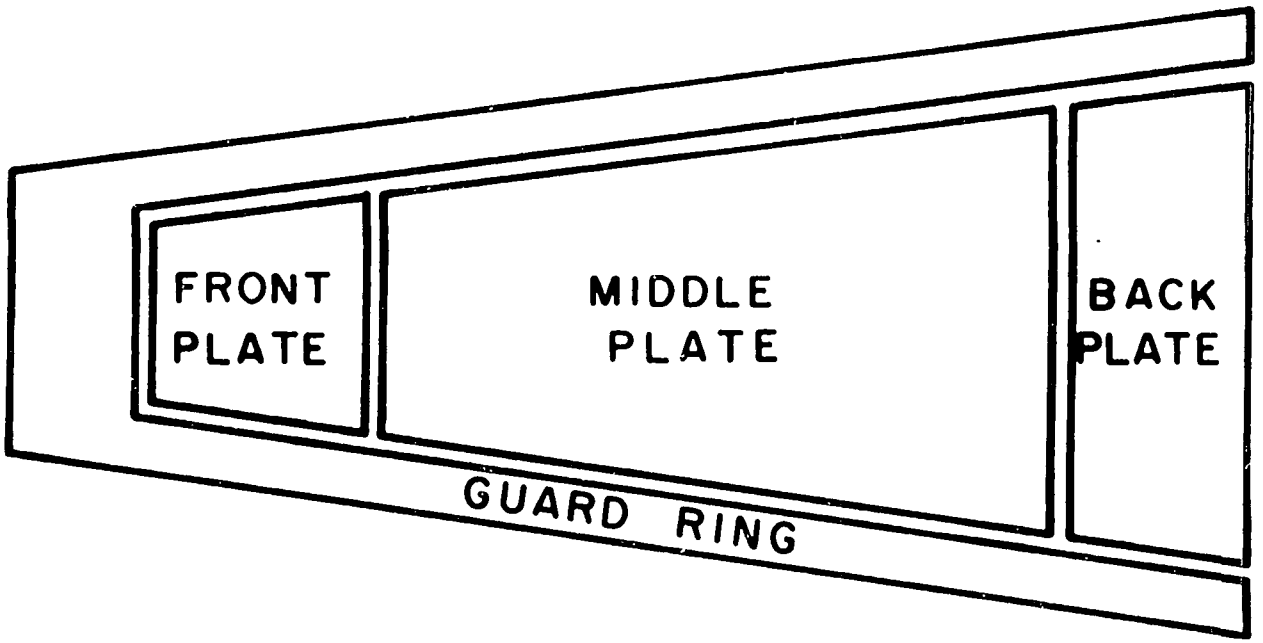

1 INCH

FIGURE 27

Particle identification curves from a calibration on Li^7, Be^9, B^{11} and C^{12} targets. The curves for Li^7 and Be^9 fold back when the recoils have sufficient energy to traverse the entire length of the first two plates.

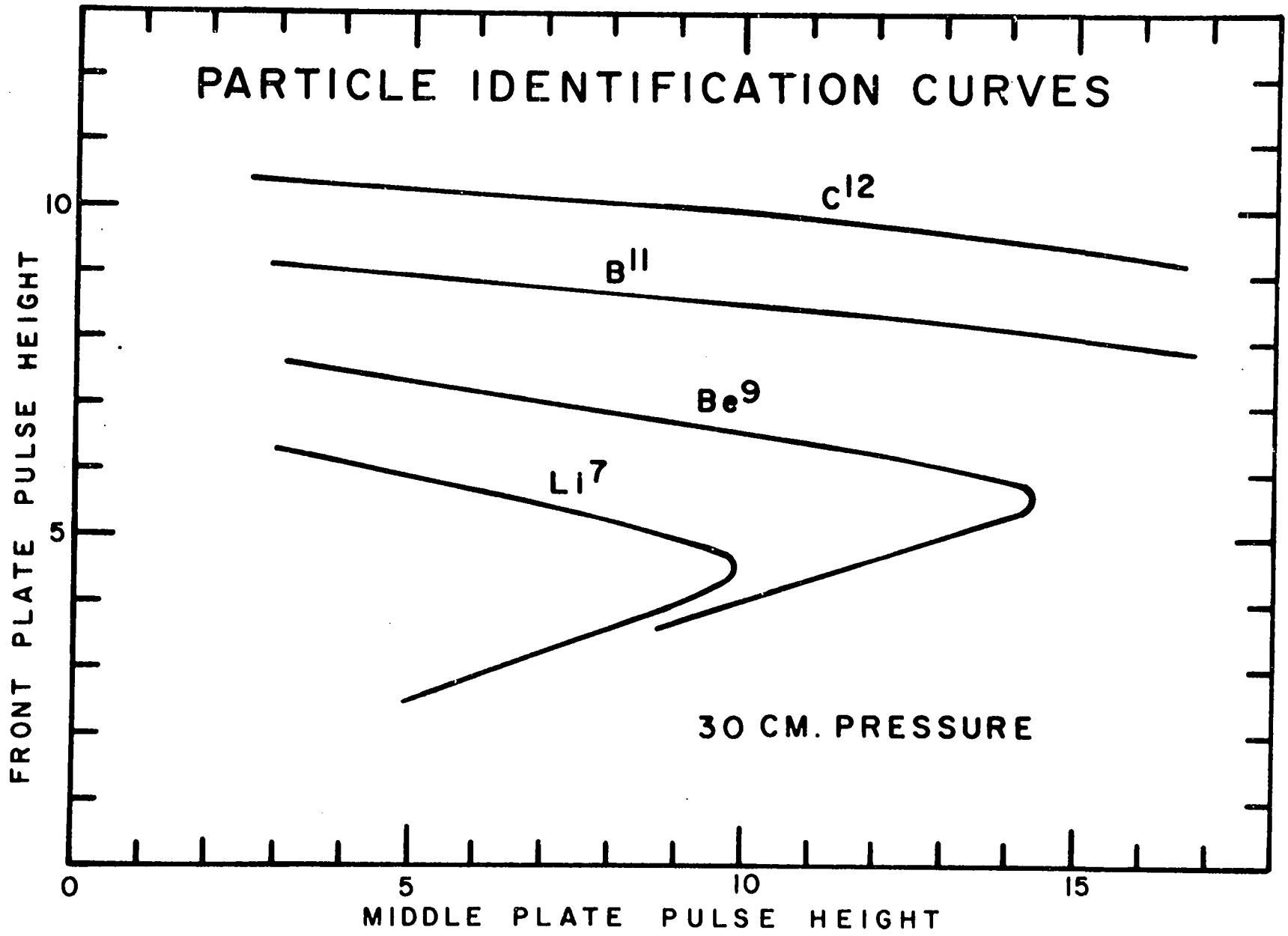
PARTICLE IDENTIFICATION CURVES
C12
B11
Be9
Li7
30 CM. PRESSURE
FRONT PLATE PULSE HEIGHT
MIDDLE PLATE PULSE HEIGHT
0
5
10
15
5
10

FIGURE 28

A typical pulse height spectrum from a carbon target for the middle plate. The counter was at 15° with respect to the beam.

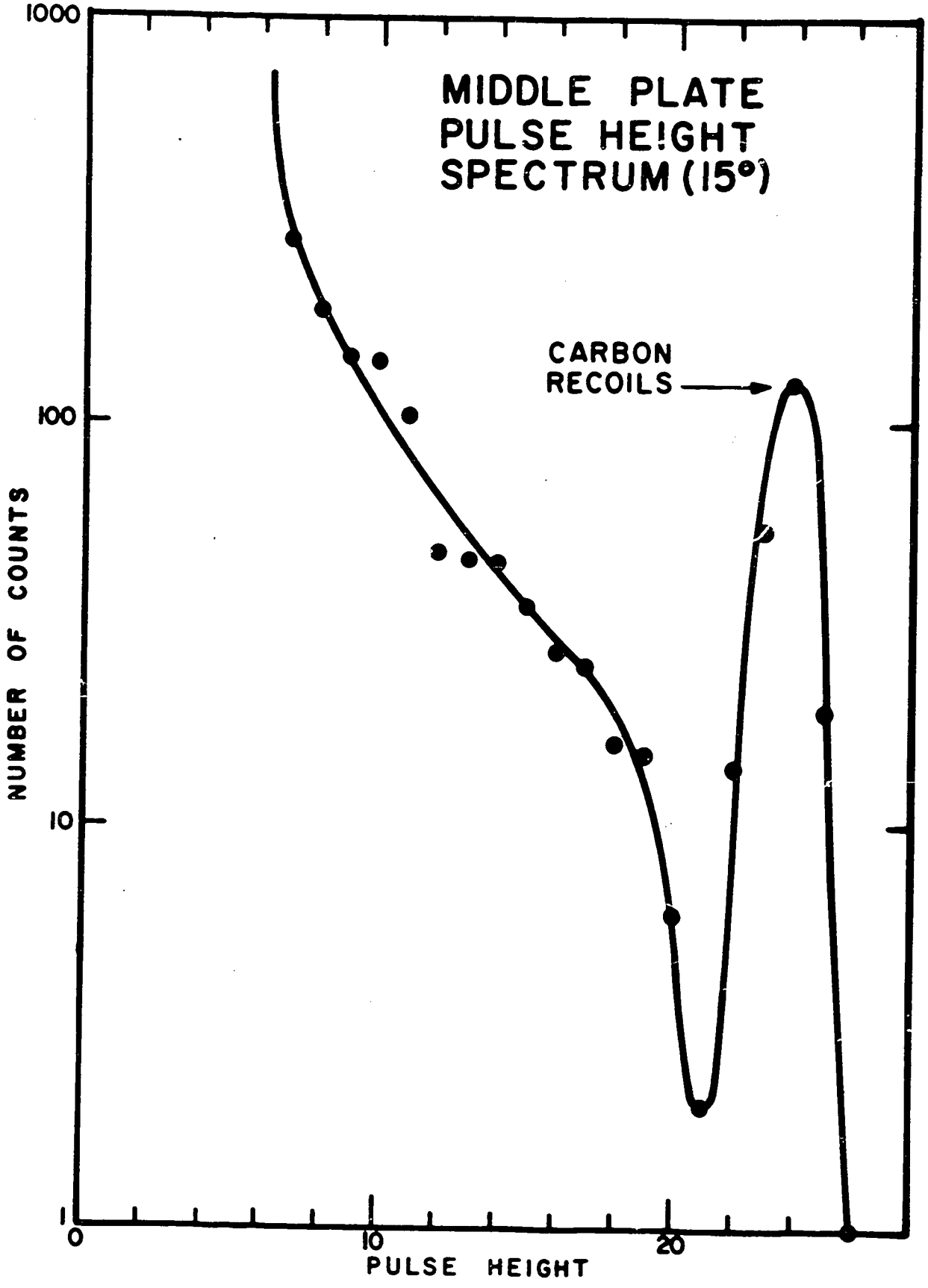
MIDDLE PLATE
PULSE HEIGHT
SPECTRUM (15°)
CARBON
RECOILS
1000
100
10
1
0
10
20
NUMBER OF COUNTS
PULSE HEIGHT

FIGURE 29

Pulse height spectra in the front plate corresponding to the middle plate spectrum given in Figure 28. The lower curve was obtained by gating the pulses from the front plate with pulses from the middle plate which came in channel 14. The peaks are identified on the basis of the calibration.

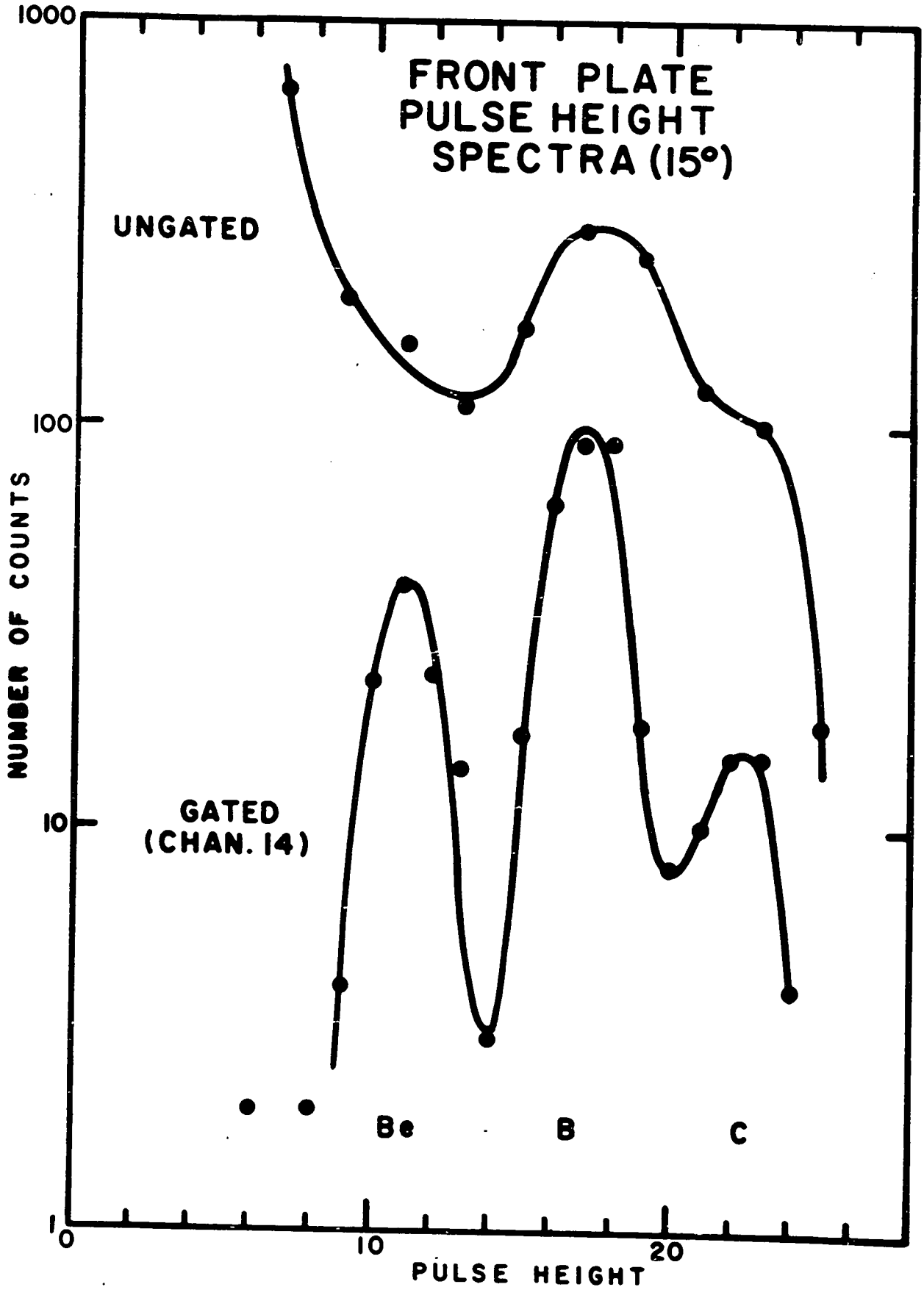
FRONT PLATE
PULSE HEIGHT
SPECTRA (15°)
UNGATED
GATED
(CHAN. 14)
Be
B
C
NUMBER OF COUNTS
PULSE HEIGHT
1000
100
10
1
0
10
20

FIGURE 30

Energy spectra of Be ions from carbon at several angles.

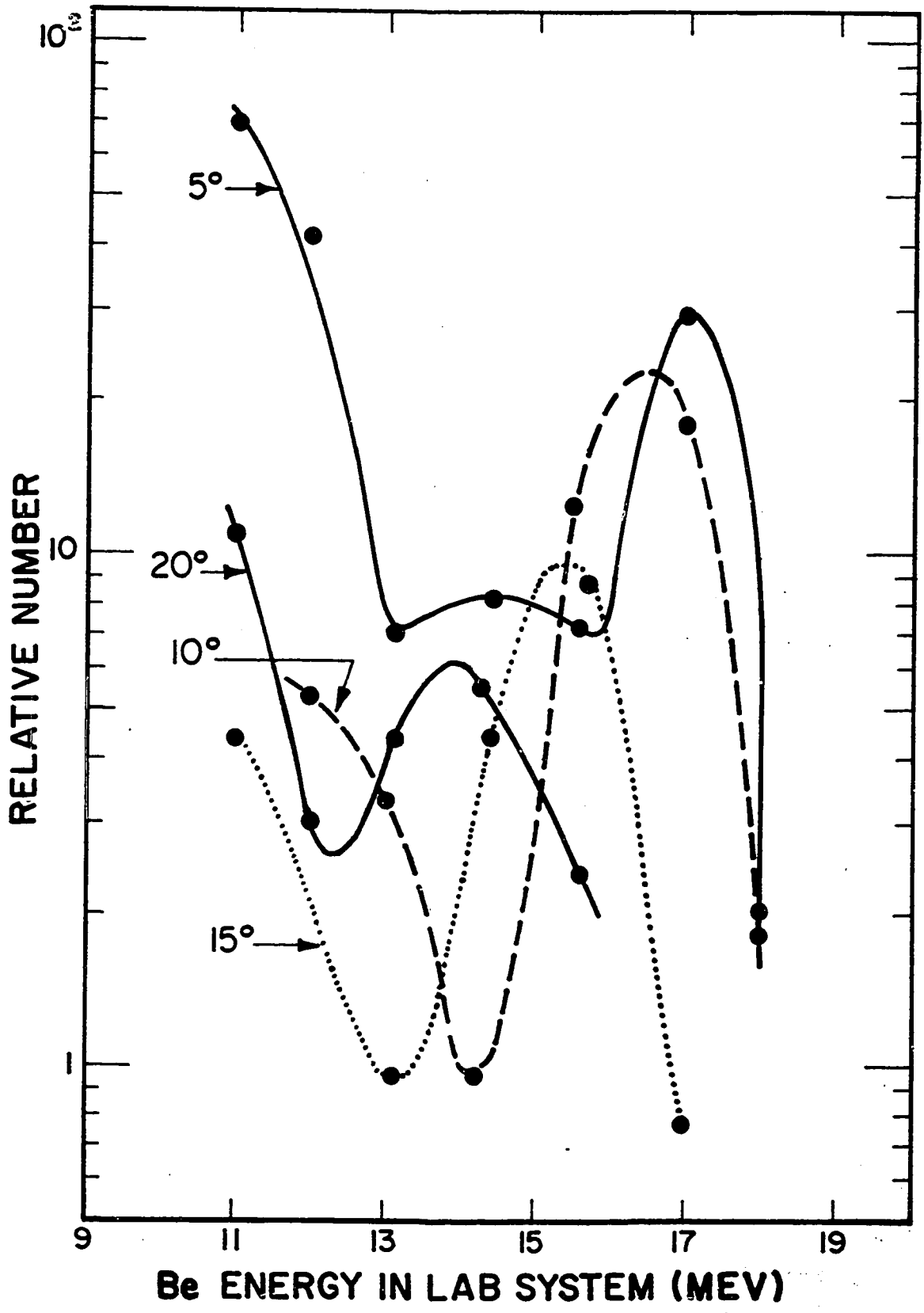
RELATIVE NUMBER
10²
10
1
5°
20°
10°
15°
9
11
13
15
17
19
Be ENERGY IN LAB SYSTEM (MEV)

APPENDIX III

A Table of Q Values and Coulomb Barrier Heights.

Table IV is a compilation of Q values and coulomb barrier heights for the (He^4, Be^7) reaction on all elements from carbon to argon. The coulomb barriers were calculated from

$$V = Z_{Be^7} Z_t e^2 / (R_{Be^7} + R_t) .$$

The subscript t refers to the target nuclide. Nuclear radii were obtained from $R = r_o A^{1/3}$ with $r_o = 1.3 \times 10^{-13}$ cm.

TABLE IV

Target Nuclide	Q (Mev)	V (Mev)
C^{12}	- 24.7	4.0
C^{13}	- 22.8	3.9
N^{14}	- 19.1	4.8
N^{15}	- 26.6	4.8
O^{16}	- 21.2	5.6
O^{17}	- 17.2	5.6
O^{18}	- 23.0	5.5
F^{19}	- 20.1	6.3
Ne^{20}	- 19.5	7.2
Ne^{21}	- 27 5	7.1
Ne^{22}	- 24.6	7.0
Na^{23}	- 22.8	7.8
Mg^{24}	- 21.6	8.6
Mg^{25}	- 18.4	8.5
Mg^{26}	- 24.3	8.4
Al^{27}	- 22.2	9.2
Si^{28}	- 21.6	9.9
P^{31}	- 20.9	10.5
S^{32}	- 17.4	11.2
Cl^{35}	- 17.9	11.8
A^{40}	- 20.9	12.2

BIBLIOGRAPHY

(1-1319) E. Baker, G. Friedlander and J. Hudis: "Formation of Be^7 in Interactions of Various Nuclei with High-Energy Protons," Phys. Rev. 112, 1319 (1958).

(2-35) J. Ball: Ph.D. thesis, University of Washington, (1958).

(3-1) R. E. Batzel and G. H. Coleman: "Cross Sections for Be^7 Production by Deuteron Bombardment of Oxygen," AECD-3799, Sept. (1953).

(4-248) H. Bethe and J. Ashkin: Experimental Nuclear Physics, New York, John Wiley and Sons, (1953).

(5-344) N. Bohr: "Neutron Capture and Nuclear Constitution," Nature 137, 344 (1936).

(6-160) G. Bouchard and A. W. Fairhall: "Production of Be^7 in 30-42 Mev He-Ion Bombardment of Oxygen, Aluminum and Copper," Phys. Rev. 116, 160 (1959)

(7-13) Compt. Rend. 220, 111-13 (1945).

(8-902) J. M. Dickson and T. C. Randle: "The Excitation Function for Be^7 Production from the Proton Bombardment of Carbon," Proc. Phys. Soc. (London) A64, 902 (1951).

(9-1659) I. Dostrovsky et al: "Monte Carlo Calculations of High-Energy Nuclear Interactions," Phys. Rev. 111, 1659 (1958).

(10-284) T. Ericson and V. Strutinski: "On Angular Distributions in Compound Nucleus Processes," Nuc. Phys. 8, 284 (1958).

(11-425) T. Ericson: "The Statistical Model and Nuclear Level Densities," Phil. Mag. 9, 425 (1960).

(12) A. W. Fairhall: Private communication, (1961).

(13-727) G. Friedlander et al: "Nuclear Reactions of Copper with 2.2 Bev Protons," Phys. Rev. 94, 727 (1954).

(14-263) G. Friedlander et al: "Disintegration of Al by Protons in the Energy Range 0.4 to 3.0 Bev," Phys. Rev. 99, 263 (1955).

(15-97) C. Gruhn: Ph.D. thesis, University of Washington, (1961).

(16-510) I. Halpern: Bull. Amer. Phys. Soc. II 5, No. 7, 510 (1960) and private communication.

(17-207) P. E. Hodgson: "The Emission of Li^8 from Cosmic Ray Induced Nuclear Disintegrations," Phil. Mag. 42, 207 (1950).

(18-1) E. L Hubbard: "Range -Energy Relation for Heavy Ions in Metals:, UCRL-9053, Jan., 1960.

(19-1322) J. Hudis and J. M. Miller: "Be^7 Nuclei as Evaporated Particles in High-Energy Reactions," Phys. Rev. 112, 1322 (1958)

(20-1665) G. Igo: "Optical Model Analysis of Excitation Function- Data and Theoretical Reaction Cross Sections for Alpha Particles," Phys. Rev. 115, 1665 (1959).

(21-905) S. Katcoff: "Energy Distribution of Li^8 Fragments from C, Al, Cu, Ag, Au and U Bombarded by 2.2 Bev Protons," Phys. Rev. 114, 905 (1959).

(22-2168) R Lindsay: "The (He^4, Be^7) Reaction in Mg, Al, Ti, Co and Cu from Threshold to 42 Mev," Phys. Rev. 120, 2168 (1960)

(23-1) J. B. Marion et al: "Tables for the Transformation Between the Laboratory and Center-of-Mass Coordinate Systems," ORNL-2574, April, (1959).

(24-953) L. Marquez and I. Perlman: "Observations on Lithium and Beryllium Nuclei Ejected from Heavy Nuclei by High-Energy Particles," Phys. Rev. 81, 953 (1951)

(25-355) B. A. Munir: "Angular Distribution of Lithium-8 Fragments in High Energy Proton Bombardments", Phil. Mag. 1, 355 (1956).

(26-18) W Nicholson et al: University of Washington, Cyclotron Progress Report (1960).

(27) L. C. Northcliffe: Private communication, (1961).

(28-1744) L. C Northcliffe: "Energy Loss and Effective Charge of Heavy Ions in Al," Phys. Rev. 120, 1744 (1960).

(29-21) Radiochemistry Group J-11: "Collected Radiochemical Procedures," LA-1721, 2nd Ed., March, (1960).

(30-175) F. S Rowland and R L Wolfgang: "Production of He^6 by High-Energy Protons," Phys. Rev 110, 175 (1958).

(31-188) S. Sorensen: "Emission of Energetic Helium and Lithium Fragments in Nuclear Explosions," Phil. Mag. 42, 188 (1950).

(32-742) S. C. Wright: "The Production of Li^8 from Various Gases," Phys. Rev. 77, 742 (1950).

(33) C. Zafiratos: Private communication (1961).

ACKNOWLEDGEMENTS

This thesis represents the cooperation of many people. It is a special pleasure to acknowledge the tremendous help extended to me by Professor A. W. Fairhall and Professor I. Halpern through many hours of consultation and discussion. Their assistance was indispensable.

I am also very much indebted to all the cyclotron personnel for their expert and ready assistance in carrying out the bombardments. It is with great appreciation that I extend my thanks to Ann Rutter for typing this thesis (twice) and to Peggy Douglass for drawing the figures.

My wife, Jo Ann, has shared with me the disappointments and successes of my work. Her patience and encouragement have contributed immeasurably to the completion of this thesis.

VITA

Charles Oliver Hower, Jr. was born May 13, 1935 in Emmett, Idaho. His parents are Charles O. and Beverly W. Hower He was graduated from Emmett High School in Emmett, Idaho in June of 1953. He received a Bachelor of Arts degree from Whitman College in September, 1956.